Mon. Not. R. Astron. Soc. **281,** 1139–1164 (1996)

Models of highly extended dust shells around R Coronae Borealis

K. N. Nagendra[1,2]★ and Chun Ming Leung[1]★

[1]*Department of Physics, Applied Physics and Astronomy, Rensselaer Polytechnic Institute, Troy, New York, 12180-3590, USA*
[2]*Indian Institute of Astrophysics, Bangalore 560034, India*

Accepted 1996 February 16. Received 1996 January 26; in original form 1995 February 8

ABSTRACT

Radiation transport models are constructed for the dust shells of the hydrogen deficient supergiant star R Coronae Borealis (R CrB). *IRAS* observations of R CrB are used as constraints in selecting the model parameters. Based on suggestions from earlier work, a double-shell model is employed as a standard configuration for R CrB. The first shell is a hot inner shell of radius 5 arcsec surrounding the central star. The second shell is a cold remnant shell which is highly extended, with a radius of 10 arcmin (derived assuming a source distance of 1.6 kpc). The two shells can be spatially separated, and can have completely different mechanisms for the heating of their dust grains. A detailed parametric study of the system is undertaken using simple power law type density and opacity for single sized grains. The models of R CrB clearly point to the configuration of a large well-separated cold dust shell surrounding a tiny hot dust shell, which supports the existing view that this extended shell is a fossil shell. However, the separation between the two shells cannot be determined purely from the radiative transfer modelling. This can still be treated as a free parameter of the system for modelling purposes. The interstellar radiation field (ISRF) incident on the outer boundary of the system plays a considerable role in explaining the 60- and 100-μm surface brightness of R CrB measured by *IRAS*. The observed constant temperature of the fossil shell, however, poses serious theoretical problems. We propose models in which the density varies as $r^{-\gamma}$ ($\gamma \approx 1.0$–1.5). The source of dust heating in our models is a combination of central star radiation and ISRF. The amorphous carbon grains seem to give better fits to the *IRAS* data than the crystalline grains do. A comparison of both the analytic models and the radiative transfer models is made, to clarify their usefulness in modelling the density and the surface brightness data of R CrB. The models are schematic in nature, and are not intended as best fitting models for the R CrB fossil shell.

Key words: radiative transfer – circumstellar matter – stars: individual: R Coronae Borealis – dust, extinction – infrared: stars.

1 INTRODUCTION

It is well known that supergiant stars with an active mass loss are also associated with large single dust shells. The existence of dust in the envelopes of several giant and supergiant stars is confirmed by infrared excess in the continuous spectrum of these stars. There are two competing models regarding the formation of dust in the R CrB class of stars. According to one model, the dust grains in the shell are basically formed by condensation of molecular gas precursors, at large distances (several tens of stellar radii) from the central star photosphere where the temperature is low enough (see e.g. Feast 1986). The other model proposes the dust forming very close to the star (see Clayton et al. 1992, 1995; Whitney et al. 1992; Whitney, Balm & Clayton 1993). These later models are based on the idea of dust formation in R CrB stars during their pulsation cycles. Further, the dust formation takes place in the outer atmospheric layers under temperatures as high as 4000 K, as a result of close proximity (2–$3\,r_*$) to the central star photosphere. The dust nucleation occurs in an atomic carbon plasma, and hence the form of carbon condensates could be quite different from the first model. However, as the dust shells are radiatively driven out from the photosphere in both the models, the temperatures of dust shells are rather small (nearly 1000 K at the dust condensation radius, down to 20 K at the

★E-mail: knn@iiap.ernet.in (KNN); Chun_Leung@mts.rpi.edu (CML)

shell boundaries). The infrared continuum radiation in R CrB arises mainly because of the emission by dust grains. Hence infrared ($\lambda > 3$ μm) continuum observations are sensitive indicators, not only of the total amount and radial distribution of dust grains in the shell, but also of their composition. Depending on the mass-loss rate at the photospheric levels, there is a wide range of characteristics and peculiarities associated with these dust shells. For example, stars with smaller mass-loss rates usually have optically thin shells and are not geometrically extended. There are some exceptions to this. The star that we have selected here for study – R CrB – is, for instance, a system with a low mass-loss rate, having an optically thin inner shell, surrounded by an optically thin, but geometrically highly extended, dust shell. The extended shell dust mass-loss rate at a distance of 1.4 arcmin from the R CrB central star is $\dot{M}_d$(1.4 arcmin) $\approx 10^{-9}$–10^{-8} $M_\odot$ yr^{-1} for $\tau_{0.55\,\mu m} \sim 10^{-4}$–$10^{-3}$, with a radiating dust mass in the range $M_d \approx 10^{-3}$–10^{-2} $M_\odot$ (see Feast 1986; Gillett et al. 1986). Such a wide range in mass-loss rate is specified because it is an estimated quantity and depends on a variety of factors, such as initial ejected mass, expansion velocity, termination period and grain models. The corresponding estimate of total mass-loss rate is $\dot{M}_t$(1.4 arcmin) $\approx 10^{-7}$–10^{-5} $M_\odot$ yr^{-1} for the ejection of a 1-$M_\odot$ hydrogen-rich envelope which expanded over a long period of 1.5×10^5 yr, terminating about 2.5×10^4 yr ago. Assuming that amorphous carbon dust constitutes the shell, this range narrows down to $\dot{M}_t$(1.4 arcmin) $\approx 10^{-6}$–10^{-5} $M_\odot$ yr^{-1} (see Gillett et al. 1986 who gave a value of 7×10^{-6} $M_\odot$ yr^{-1}). The present mass-loss rate in the fossil shell seems to be even smaller compared to the inner compact shell. The infrared astronomical satellite (*IRAS*) observed several such objects, characterized by significant 100-μm flux, but unusually large 100-μm extended emission (meaning intensity distribution extending up to very large distances from the central star position). It is important to note that detection of such extended emission was possible owing to disc-resolved intensity measurements, made with beam sizes much smaller than those normally used in disc-integrated flux measurements.

The R CrB phenomenon – the strong decline in apparent brightness, caused by new dust formation or occultation events – is a well–explored topic (see Feast 1975, 1986, 1990; Clayton 1996). From the irregularity of the decline, the hot dust distribution around the central star appears to be clumpy. However, for modelling purposes, it is reasonable to assume that this hot dust forms a spherical shell. We are mainly concerned in this paper about the vast cold dust shell discovered by Walker (1985) with *IRAS*, and modelled by Gillett et al. (1986) using *IRAS* data. This shell appears to represent an episodic mass-loss event in the past, which discontinued during the evolution of central star. Rao & Nandy (1986) also predicted the existence of a cold (30 K) dust component of emission in R CrB, which they suggested as the remnant of a previous evolutionary stage. It is worthwhile to study this remnant shell because of its relevance to mass loss in late-type supergiant stars. The extended shell of R CrB was modelled by Gillett et al. (1986) using the *IRAS* flux spectrum and surface brightness data, to derive the parameters such as total dust mass and mass-loss rate in the extended shell. The question of whether the extended shell of R CrB is part of an ongoing mass-loss process, or simply a colder remnant (fossil dust) of earlier 'episodic mass-loss' events, is still not clear. Detailed radiation hydrodynamic modelling, starting from evolutionary status of asymptotic giant branch stars is required to answer this question. Using an advanced deconvolution procedure, Hawkins & Zuckerman (1991) made a detailed modelling of the *IRAS* surface brightness observations on planetary nebulae (PN). They have shown that the 60-μm profiles are more sensitive to density distribution in the dust shell, than to the dust temperature. It is clear from their studies that model fits to the spectral and spatial distribution of infrared emission data provide a better constraint on model parameters, than the fits to flux data alone. In a recent paper, Clayton et al. (1992) have shown that the inner radius of a hot dust shell could be much less than the normally assumed carbon dust condensation radius in R CrB. This important point has to be taken into account in modelling efforts of R CrB more detailed than those presented in this paper.

The most comprehensive analysis to date, regarding resolved circumstellar dust shells observed by *IRAS*, is made by Young, Phillips & Knapp (1993a,b). A model fit is obtained to the *IRAS* survey data of R CrB by Young et al. (1993a), using an unresolved source surrounded by an isothermal dust shell resolved in 60 and/or 100 μm. The success of these model fits in R CrB and other systems, is convincing as to the reality of these extended structures actually being associated with central stars. In their second paper, Young et al. (1993b) show that in several systems, the average dust temperature in the outermost regions of the shells is approximately 35 K. They also show that in some cases, the shells are detached from the central star, and that the dominant source of dust heating, up to radial distances of 0.5 pc, is the central star radiation field, whereas an external source indeed dominates the dust heating for radial distances beyond 1 pc. Our conclusions regarding dust heating in the extended shells of R CrB support the conclusions of Young et al. (1993b) for this system. Recently Van der Veen et al. (1994) have studied the dust shells around high latitude supergiants. These authors combined their submillimetre observations with near-infrared as well as *IRAS* data, and fitted them with optically thin models. They showed that a large fraction of IR excess originates from a hot dust shell close to the star, and concluded that the emission longward of 60 μm cannot be explained with only one dust shell, and that IR excess at far-infrared and sub-millimetre wavelengths is produced by a second colder dust shell. They suggested that the second cold dust shell could be a remnant shell through a study of the mass-loss history of several supergiants (Van der Veen, Trams & Waters 1993). It is important to note that Rowan-Robinson (1982) had already employed the scenario of double shells in modelling Type II OH-IR sources. He suggested that the second detached shell could represent a previous phase of ejection by the star.

Our purpose in this paper is to re-examine the modelling of the R CrB data obtained by *IRAS*, through a self-consistent radiative transfer approach. We do not attempt to provide best fits to the observed data, but concentrate on general characteristics of the modelling, the procedures required and the difficulties in general that arise in modelling such highly extended shells. However, through our independent approach, we confirm qualitatively the conclu-

sions reached by the above mentioned authors regarding the nature and physical properties of the R CrB cold dust shell.

This paper is organized into three sections. In Section 2 we present the results of Analytic Modelling (AM) and Radiation Transport Modelling (RTM) of R CrB, through a two-shell model approach. The model parametrizations in AM and RTM are tabulated. Our convolution procedure is described in Appendix A. We show the dependence of results (flux density in all four *IRAS* wavelength bands plus intensity in the 60- and 100-μm bands) on several important model parameters, and demonstrate how the fit to surface brightness constrains the free parameters to narrow ranges, unlike a fit only to the flux density. Each subsection deals with the effect of variation of a given single model parameter. But one common (best fit or reasonable fit) model forms the basis for all the subsections as a 'median model'. In Section 3, we summarize the main conclusions of our studies. Throughout the paper, the quantities that are specific to the extended shell are distinguished with an argument 'ext' for clarity.

2 DISCUSSION OF MODEL RESULTS

In this section we discuss the analytic model results, and compare them with the radiative transfer model results. The equations required for AM are given in Gillett et al. (1986), so we do not present them here. We assume a power-law type variation of the dust number density in the circumstellar shells of R CrB:

$$n(r)=n_0(r_0/r)^{\gamma}\ \mathrm{cm}^{-3}, \tag{1}$$

where the index γ is the density exponent, r_0 a reference radius and n_0 a normalization constant. We can express n_0 in terms of the mass-loss rate $\dot{M}_{\mathrm{d}}$ and the velocity of the dust wind at r_0. We follow the procedure described in Sopka et al. (1985) for this purpose. The dust absorption coefficient $\kappa(\lambda)$ is assumed to vary according to a power law:

$$\kappa(\lambda)=\kappa_0(\lambda_0/\lambda)^m\ \mathrm{cm}^2\ \mathrm{g}^{-1}, \tag{2}$$

where m is the opacity exponent, and $\kappa_0=\kappa(\lambda_0)$ is the absorption coefficient at reference wavelength λ_0, and given by

$$\kappa(\lambda_0)=\frac{Q_{\lambda_0}\pi a^2}{\rho_{\mathrm{d}}(4\pi a^3/3)}\ \mathrm{cm}^2\ \mathrm{g}^{-1}, \tag{3}$$

where Q_{λ_0} is the absorption efficiency of the dust particle at wavelength λ_0.

2.1 Model parametrization in AM and RTM

In Table 1 we list the model parameters required for AM and RTM. Conventional notation is employed. Most of the free parameters are common for both of the methods. However, there are essential differences in the way that some of the parameters are used. The RTM analysis is not much different from the AM analysis as far as geometry (two-shell model) is concerned. The convolutions on intensities are also performed in exactly the same manner in both cases. The differences between AM and RTM are as follows.

(i) The temperature structure $T(r)$ is assumed in AM, and given by the equation

$$T(r)=T_*[(r_*/2r)^2+6.9\times10^{-13}C]^{1/(4+m)}, \tag{4}$$

in the conventional notation. On the other hand, $T(r)$ is computed self-consistently in RTM by solving the radiative transfer equation and energy balance equation simultaneously and iteratively. The rate of convergence depends on the initial guess for $T(r)$. The constant quantity C represents the strength of the dust heating by the external interstellar radiation field (ISRF). See Leung (1976), Egan, Leung & Spagna (1988) and Doty & Leung (1994), for a discussion of the method of solution, details of the coding and applications respectively. The $T(r)$ computed from equation (4) can be used as an initial guess, with m and C(ext) values derived approximately by the corresponding best fit AM. We have found this procedure to be very useful in practice.

(ii) In AM, although a spatially independent dust heating source can be assumed through a choice of $C(\mathrm{ext})\neq0$, finer details such as the relative strength and the frequency dependence of this external source are not relevant. Similarly, in RTM, this heating source is assumed to be the local diffuse ISRF incident on the outer boundary. We use the ISRF data for the solar neighbourhood. Since R CrB is well above the galactic plane, using ISRF in the vicinity of the Sun as a measure means a slight overestimation of the local ISRF spectrum. However, more significant is the question of the possible presence of an intense radiation environment around R CrB. Based on *IRAS* observations of the nuclear bulge of the nearest spiral galaxy M31, Soifer et al. (1986) argue that the ISRF in the galactic bulge of our Galaxy could also be very strong (see Gillett et al. 1986). Since the local ISRF is used as a boundary condition, theoretically computed flux and surface brightness results depend much more sensitively on its strength and frequency dependence. The dust heating from ISRF is caused mainly by its UV component.

(iii) The normalization constants r_0, $n_0(r_0)$ and $T_0(r_0)$ derived in AM can be used advantageously in RTM also. However, the total optical depth, defined as

$$\tau_\lambda(r)=\int_{r_{\max}}^{r} Q_\lambda\pi a^2 n(r)\,\mathrm{d}r, \tag{5}$$

is a more useful free parameter in RTM.

(iv) In computing brightness profiles in AM, we inherently assume that the emission originates locally in an extended shell in thermal equilibrium with the central star radiation. An inner hot dust shell of radius 5 arcsec around the central star is employed to model the point-source-processed flux densities. Hence both these shells are treated in a completely independent manner. However, the diffuse radiation field at every point within the system depends on contributions from the central star, the inner hot shell and the extended shell. The respective parameters enter the RTM modelling naturally, as the whole system is considered.

(v) The difference between the AM and the RTM solutions increases as the dust optical depth increases, since AM is based on the optically thin approximation.

2.2 AM of R CrB

We now discuss some AM results; (a) to show the similarities between the AM and RTM approaches, and (b) to show that for optically thin dust shells, both AM and RTM give similar results. Indeed, we find that in general, AM solutions which are much less expensive to compute can be used to establish initial bounds on a number of free parameters, so that a trial-and-error procedure with RTM (which is more expensive) can be avoided. In this way AM can act as an initialization step to RTM.

We select a set of model parameters for R CrB (see Table 1), close to those suggested by Gillett et al. (1986). In Fig. 1(a) we show by triangles the observed flux density in the *IRAS* bands measured in the point-source mode. The flux density measured with a 24 arcmin diameter beam is shown by circles. The AM flux density is computed by using equation (4) in the appendix of Gillett et al. (1986), on which spectral convolution is performed as described in the appendix. The radius of the inner hot shell is 5 arcsec. This is the shell usually detected in the near-infrared by ground-based measurements (cf. Stein et al. 1969; Forrest, Gillett & Stein 1972). The angular diameter of the outer extended shell is taken as $R=20$ arcmin, at a distance of $D=1.6$ kpc. From Fig. 1(a) we see that all the three models produced nearly the same flux density $\tilde{F}(\lambda)$. In Fig. 1(b) we show the observed (60-/100-μm) intensity ratio as a function of apparent position p (expressed in units of R) on the visible disc. Note that the observed ratio remains nearly constant across the extended cold shell, comprising the region $r>1$ arcmin (or $p>0.1$). The lines show the theoretical intensity ratio $[\tilde{I}(60\ \mu\text{m}, p)/\tilde{I}(100\ \mu\text{m}, p)]$ computed by AM. The theoretical ratio remains nearly constant across the entire disc. The constancy of the intensity ratio implies that the

Table 1. Model parametrizations in AM and RTM.

parameter	AM	RTM	comments
D=Distance to the source	1600 pc	1600 pc	from Gillett et al. (1986)
R=Radius of the source	1.54 10^{19} cm	1.54 10^{19} cm	corresponds to 10′ at 1600 pc
$\Omega(\lambda_0, T_0)$=solid angle subtended by the source	1.43 10^{-10} Sr	1.43 10^{-10} Sr	estimated using $\lambda_0 =$ 100 μm and $T_0 = 30$ K
L_* = central star luminosity	1.04 $\times 10^4$ $L_\odot$	1.04 $\times 10^4$ $L_\odot$	from Gillett et al. (1986)
T_* = central star temperature	7000 K	7000 K	from Gillett et al. (1986)
r_* = central star radius	4.824 10^{12} cm	4.824 10^{12} cm	from Gillett et al. (1986)
$V_d(ext)$ = velocity of dust wind	25 km S^{-1}	25 km S^{-1}	estimated quantity; assumed as constant
$M_t(ext)$ = total mass of dust and gas	$< 0.5\ M_\odot$	$< 0.5\ M_\odot$	estimated quantity
$\dot{M}_d(r_0, ext)$ = mass loss rate at r_0	estimated quantity; model dependent	Estimated quantity; model dependent	see Gillett et al. (1986); and Table 3
r_{min} = inner radius of inner shell	84.36 r_*	84.36 r_*	dust formation radius
r_{max} = outer radius of inner shell	2.67 10^4 r_*	2.67 10^4 r_*	from Gillett et al. (1986)
γ = density exponent for inner shell	2.0	2.0	steady state mass-loss
T_1 = dust temp. at inner boundary of inner shell	900 K, from optically thin energy balance	from RT + actual energy balance	Gillett et al. (1986); and Leung (1976)
$T_{min}(ext)$ = dust temp. at inner boundary of *ext* shell	*ext* shell is assumed as isothermal, eg. 30K	from RT + actual energy balance	Gillett et al. (1986); and Leung (1976)
$r_{min}(ext)$ = inner radius of fossil shell	0.14 R cm = 1.4′	0.14 R cm = 1.4′	location of fossil shell see Gillett et al. (1986)
$r_{max}(ext)$ = outer radius of fossil shell	R cm = 10′	R cm = 10′	from IRAS data; see Gillett et al. (1986)
$\gamma(ext)$ = density exponent for *ext* shell	2.0	1.9	steady state mass-loss; see Gillett et al. (1986)

Table 1 – *continued*

parameter	AM	RTM	comments
r_0 = reference radius	1.4′	1.4′	from Gillett et al. (1986)
T_0 = reference temperature	30 K	30 K	from Gillett et al. (1986)
λ_0 = reference wavelength	100 μm	100 μm	from Gillett et al. (1986)
$\kappa(\lambda_0)$ = reference opacity	400 $cm^2\ gm^{-1}$	400 $cm^2\ gm^{-1}$	amorphous carbon grains
ρ_d = physical density of dust	3 gm cm^{-3}	3 gm cm^{-3}	from Gillett et al. (1986)
a = dust particle radius	0.05 μm	0.05 μm	medium sized grains
m = opacity exponent for *ext* shell	1.0 (amorphous carbon)	1.0 (amorphous carbon)	fits better than crystalline carbon
$\sigma_{b,\ 100\ \mu m}$ = beam size parameter at 100 μm	0.225	0.225	from IRAS catalogue
$\sigma_{b,\ 60\ \mu m}$ = beam size parameter at 60 μm	0.125	0.125	from IRAS catalogue
$C(ext)$ = strength of external heating by *ISRF*	0 for $T(ext)$ = 30 K 4-10 for arbitrary $T(r, ext)$	15 for standard RTM	solar neighbourhood *ISRF*; see Mathis et al. (1983)
$C_2(ext)$ = density enhancement parameter	10	5 for standard RTM	dust accumulation by mass-loss episodes
$\tau_{0.55\mu m}$ = optical thickness of inner hot shell	not used in AM	0.22	inner shell is optically thin
$\tau_{0.55\mu m}(ext)$ = optical thickness of *ext* shell	not used in AM	10^{-3}	*ext* shell is optically very thin
boundary condition at inner radius of hot shell	not necessary for AM	Planckian emission of central star	as boundary condition essential for RTM
boundary condition at outer radius of *ext* shell	not necessary for AM	$C(ext) * I_{\nu,ISRF}(\lambda)$	as boundary condition essential for RTM

dust temperature is independent of distance from the central star – this is the most important feature of the R CrB data on the extended shell. If the dust in the extended shell is heated only by radiation from the central star, the dust temperature should not be constant because of geometric dilution of stellar radiation. In Fig. 1(c) we show the 60-μm brightness distribution from AM results. The filled triangles represent disc-resolved, unprocessed, in-scale *IRAS* data measured with a 1.5×5 arcmin^2 beam. In Fig. 1(d) an analogous measurement made with a 3×5 arcmin^2 beam in the 100-μm band is shown by filled squares. The open triangles and open squares represent the corresponding point-source-processed data in these two bands.

We employ unprocessed integrated flux density, in-scan surface brightness and intensity ratio data (see Gillett et al. 1986) for fitting our models. We perform beam convolution on the AM theoretical profiles as discussed in Appendix A. For a Gaussian beam pattern, our approach is equivalent to the approach of Gillett et al. (1986, their fig. 3) since our Gaussian beam function clearly resembles their PSR function in shape and width. The curves in Fig. 1(c) represent intrinsic (as yet spectrally and spatially unconvolved) profiles. The three curves correspond to three different constant temperatures of the extended shell. In obtaining these profiles, we have used $C_2(\text{ext}) = 10$, i.e., we have enhanced the density contrast throughout the extended shell (1.4 arcmin $< p <$ 10 arcmin), as compared with the density distribution function extrapolated from the 5 arcsec inner shell. We will later show that this density contrast in the extended shell is required to fit the *IRAS* data, particularly the 100-μm data. Such a detached shell should maintain a constant mass-loss rate, C_2(ext) times larger than the ongoing mass-loss rate prevalent in the inner hot shell, if we assume the same velocity of expansion V_d(ext) in both of the shells. This scenario, although plausible, is not standard since the distance to which the remnant ext shell has moved, should depend upon actual evolutionary details of the system, and should not be chosen arbitrarily to fit the surface brightness data. In this paper, we have employed this apparent location of the remnant shell (formed by an earlier mass-loss episode) as a free parameter, to show that a series of models are possible depending on this parameter alone. In Figs 1(e) and (f) we show the corresponding cases of Figs 1(c) and (d), but after those theoretical intrinsic profiles have been spectrally and spatially convolved with the respective spectral (G) and beam (S) response functions. The spectral convolution involves the intrinsic profiles at several other wavelengths in the spectral band, for which the spatial

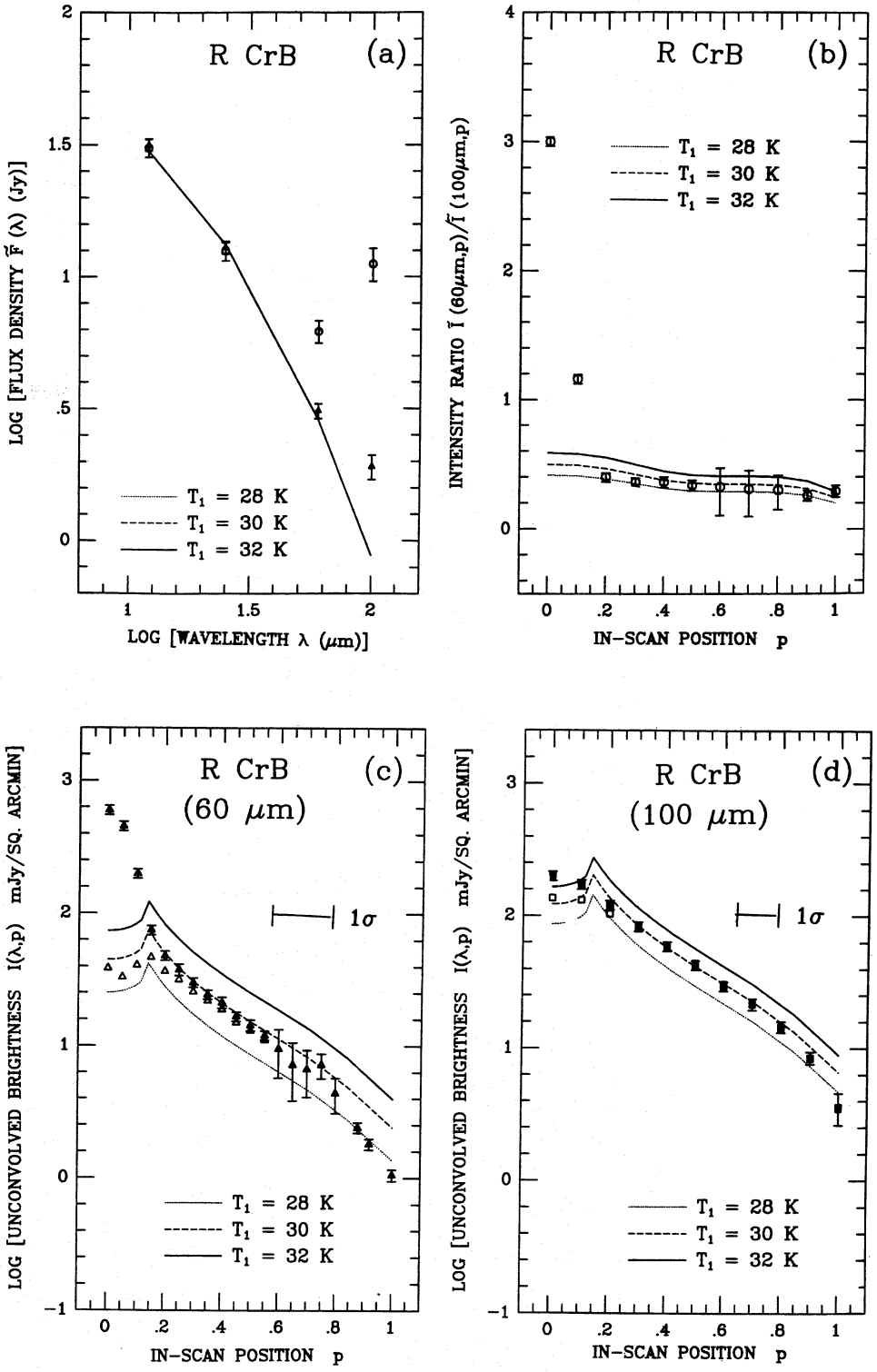

Figure 1. Analytic isothermal models of R CrB. Symbols represent observations, and the curves represent theoretical models. (a): *IRAS* flux spectrum. Triangles – point source processed flux density. Circles – integrated flux density observed with a 24 arcmin beam. (b): unprocessed 60- to 100-μm intensity ratio, plotted as a function of beam position p on the visible disc, expressed in terms of the extended shell radius R (chosen as 10 arcmin). This normalized impact parameter p can be converted to arcmin by multiplying p with 10. The curves represent isothermal analytic model fits corresponding to three different constant temperatures of the extended shell. (c): 60-μm surface brightness. Open triangles – point-source processed data. Filled triangles – unprocessed data. (d): 100-μm surface brightness. Open squares – point-source processed data. Filled squares – unprocessed data. Models are intrinsic (unconvolved) profiles for a prescribed T_1(ext). (e) and (f): same as (c) and (d) except for spectral and spatial convolution performed on the intrinsic profiles. (g): physical parameters of isothermal models. The density profile $n(r)$ is expressed in arbitrary units. $\tau(r)=\tau_{0.55\,\mu m}$(ext, r) is the optical depth scale, and $T(r)=T$(ext, r) is the temperature profile.

dependences are quite different. The spatial convolution, however, smooths out the spatial features such as the one at the inner boundary of the fossil shell (the kink at 1.4 arcmin), basically due to spatial coupling of the emission from nearby lines of sight covered inside the area of individual beam integration. The models shown in Fig. 1 are isothermal models. When the dust temperature distribution is computed using equation (4), the free parameters required to fit the observations will be different. In that case, the temperatures in most parts of the fossil shell turn out to be smaller than in isothermal models. For non-isothermal models, we require $C(\mathrm{ext})=4$–10 to match the observed data.

2.3 RTM of R CrB

The model parameters required for RTM are listed in Table 1. All the model parameters have the same values as in the

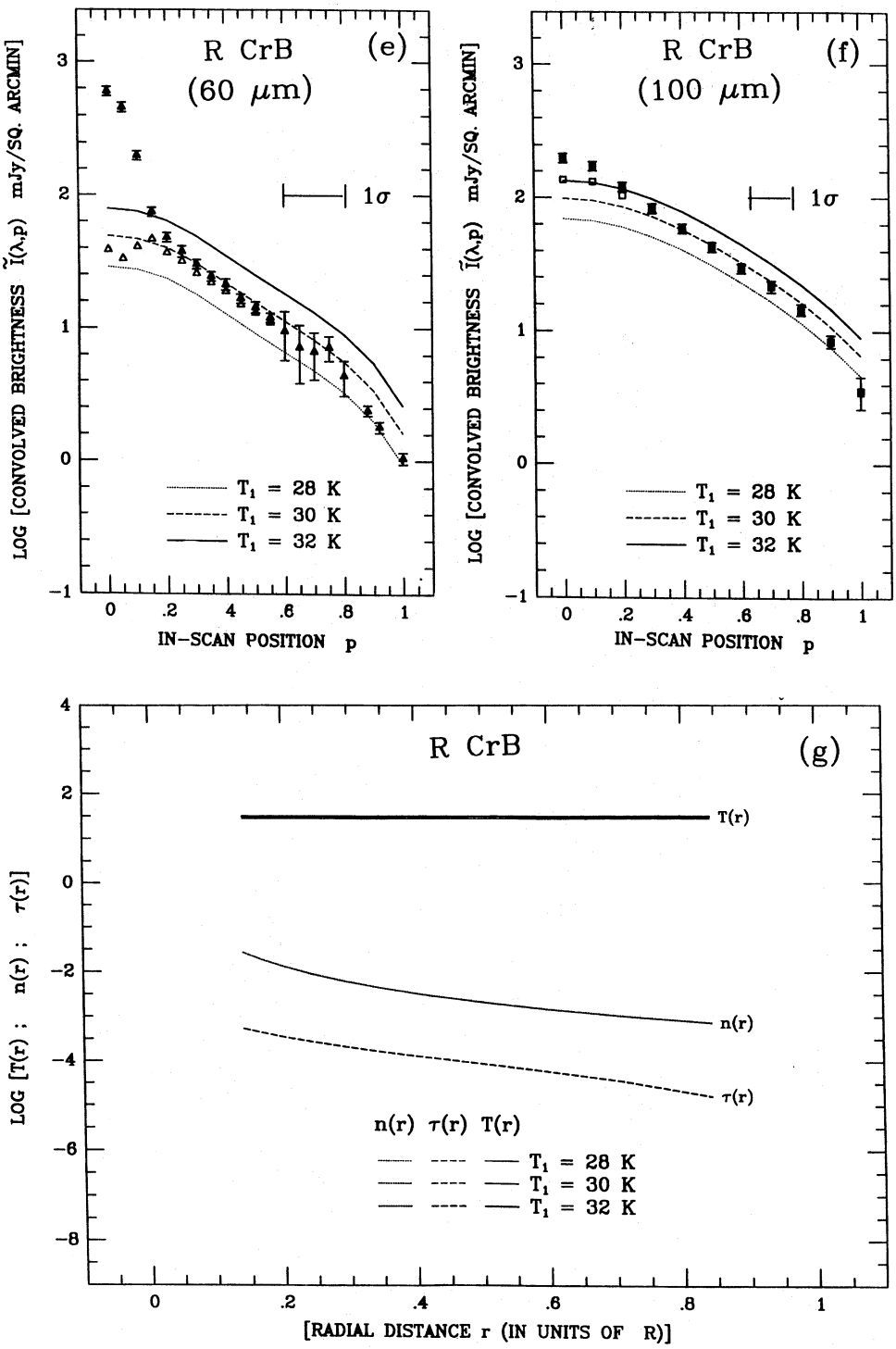

Figure 1 – *continued*

case of AM, unless stated otherwise. In addition, the following input parameters are required: $\tau_{0.55\,\mu m}$, the total optical depth at 0.55 μm and values of $I_{\nu,\mathrm{ISRF}}(\lambda)$ in the solar neighbourhood. For the RTM, we employ an 'RTM standard model' to compute the models discussed in all the Figs 2–9. The RTM standard model has the following set up, unless mentioned otherwise: inner compact shell [$\tau_{0.55\,\mu m}=0.22$, $T_1=900$ K, $\gamma=2$, $m=1$, $C=0$, $C_2=1$] and the ext shell

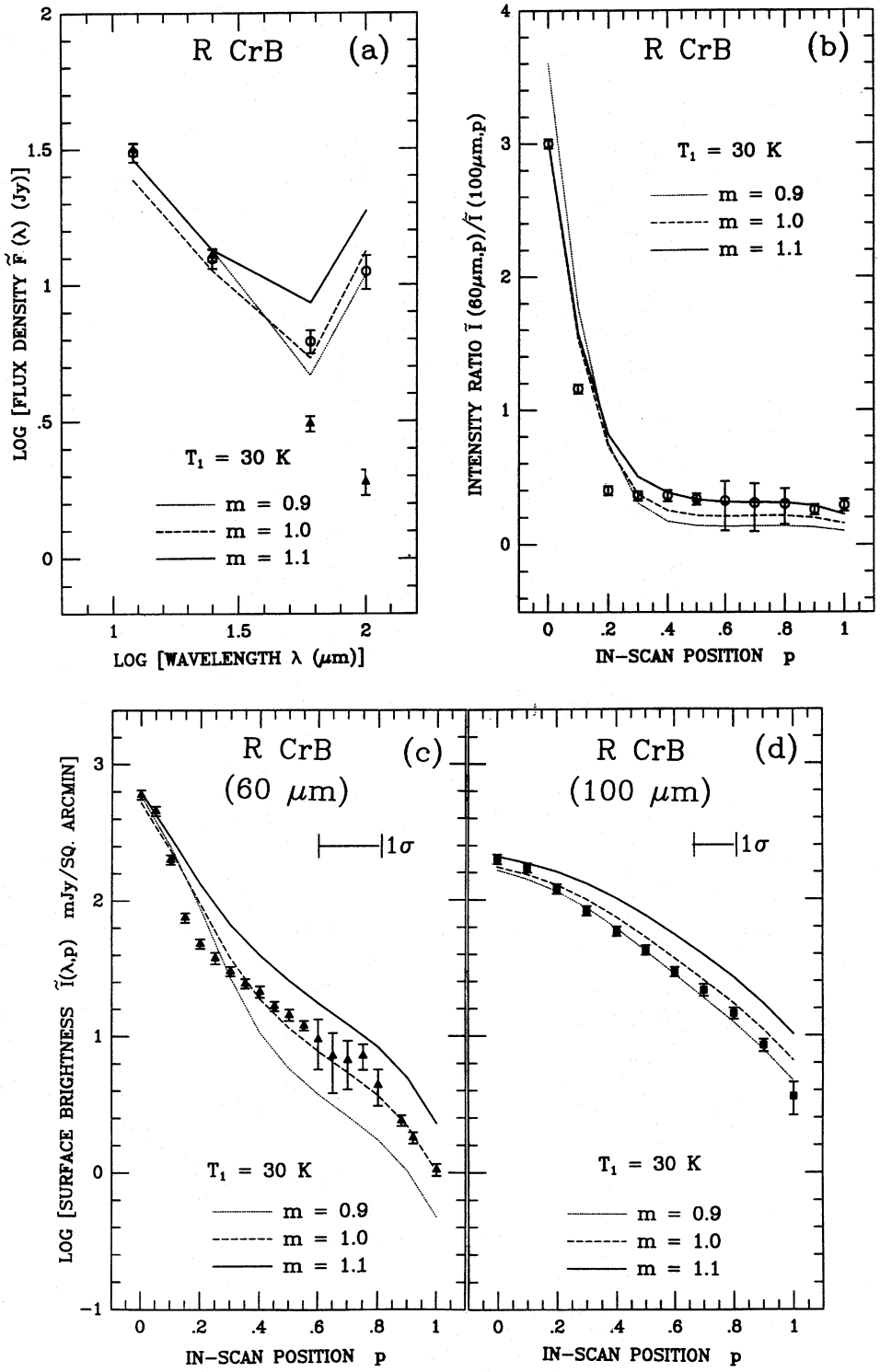

Figure 2. Radiative transfer models for *IRAS* observations of R CrB. The symbols and data points have same meaning as in Fig. 1. The lines represent model fits to the *IRAS* data. The opacity index m is the free parameter. (a) and (b): the flux density and intensity ratio respectively. (c) and (d): the radiative transfer models of R CrB surface brightness at 60- and 100-μm. The models represent spectrally and spatially convolved profiles. (e): the theoretically derived physical quantities, $n(r)$, $\tau(r)$ and $T(r)$ are shown for both the compact and the extended shell.

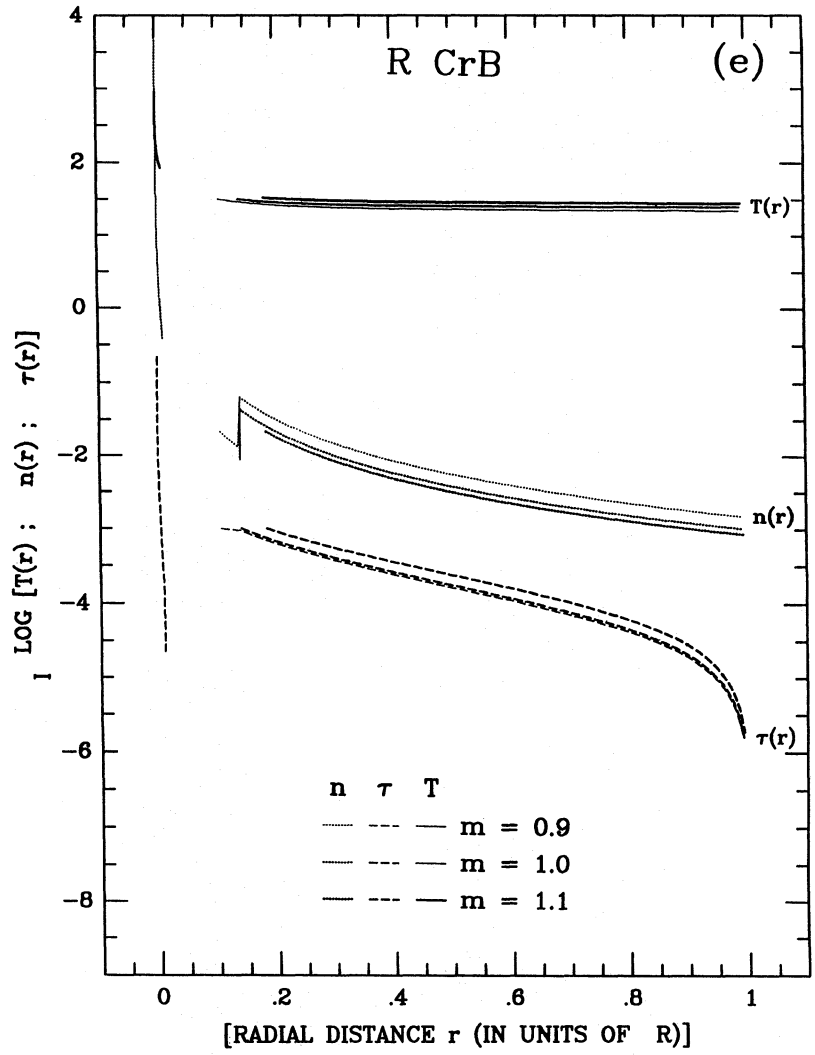

Figure 2 – *continued*

$[\tau_{0.55\,\mu m}(\text{ext}) = 10^{-3}$, $T_1(\text{ext}) = 30$ K, $r_1(\text{ext}) = 1.4$ arcmin, $\gamma(\text{ext}) = 1.9$, $m = 1$, $C(\text{ext}) = 15$, $C_2(\text{ext}) = 5]$. The external boundary condition given is a radiation field of strength $C(\text{ext}) \times I_{\nu,\text{ISRF}}(\lambda)$. We now discuss the effect of variation of the individual model parameters.

2.3.1 *Effect of variation of the opacity exponent m of the extended shell*

In Fig. 2 we present a series of RTM models using the RTM standard model, but with different m and compare them with the results of AM. In Fig. 2(a) we show the flux density data. The data points have the same meaning as in Fig. 1(a). The inner boundary condition for the ext shell is the diluted radiation of the compact shell. Increasing the size of the compact shell enhances the long-wavelength flux density. The model parameters used for the three cases ($m = 0.9$, 1.0, 1.1) shown in Fig. 2, are closer to the best-fitting model parameters suggested by Gillett et al. (1986). It can be seen that the results are quite sensitive to the opacity index m. Depth dependence of some physical parameters in the two-component RTM model are plotted in Fig. 2(e). The variation of m indirectly affects the equilibrium temperature distribution in the extended shell. Increasing m from 0.9 to 1.1 strongly increases the 60- and 100-μm emission. The purpose of Fig. 2 is to show the sensitivity of model fits to the grain type. We conclude that absorption by amorphous, instead of crystalline, carbon dust provides a narrow range for the other model parameters. However, it is hard to suggest observational consequences for a particular choice of m.

2.3.2 *Effect of position r_1(ext) of the extended shell*

We present a series of models by using the RTM standard model, and changing only $T_1(\text{ext})$, the inner boundary temperature of the extended (fossil) shell. The position of the inner edge of the extended shell $r_1(\text{ext})$ is computed from $T_1(\text{ext})$, which is actually given as input. In Fig. 3 we show the results for models with three different locations of the extended shell: $r_1(\text{ext}) = 1.4$, 0.4 and 0.12 arcmin corresponding to temperatures $T_1(\text{ext}) = 30$, 50 and 80 K respectively. Compared to the results of the $T_1(\text{ext}) = 50$ K model, moving out the extended shell leads to a decrease in the 12-

and 25-μm fluxes because dust near the inner edge of the fossil shell cannot be heated sufficiently to emit in the 12- and 25-μm bands. When the fossil shell is moved inwards, the 12- and 25-μm fluxes do not change anymore for locations closer than that corresponding to the $T_1(\text{ext}) = 50$ K case. Since the column density of cold dust decreases, both the 60- and 100-μm fluxes and intensities decrease in constant proportion, in the outer parts ($p > 0.4$) of the shell. The dust temperature distributions in the two cases, indentified by $T_1(\text{ext}) = 80$ K and $T_1(\text{ext}) = 30$ K, do not differ

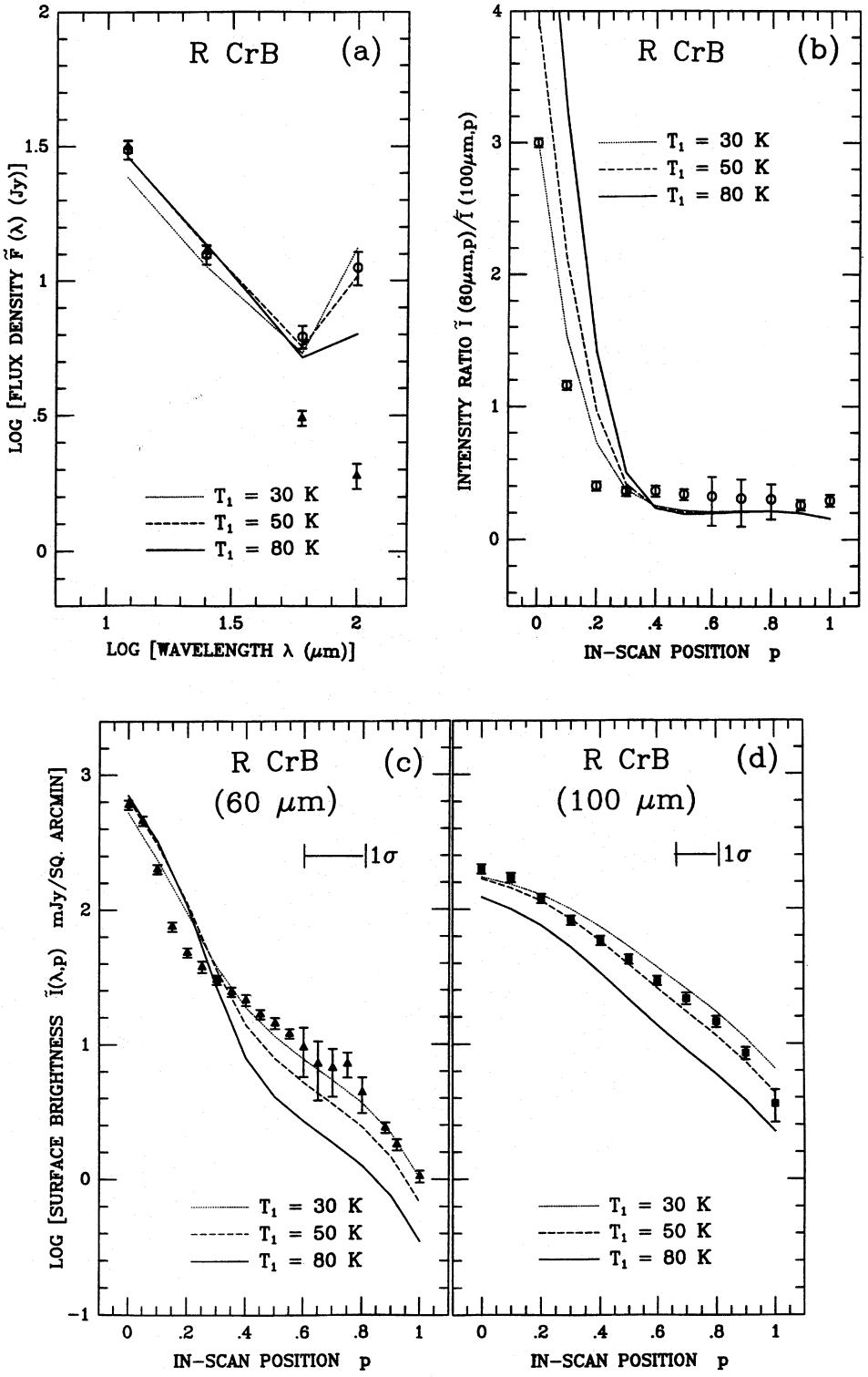

Figure 3. Models of R CrB when the extended shell is positioned at different distances from the central star. $T_1(\text{ext})$ (=30, 50 and 80 K) is the free parameter of the problem. The further away the shell is, the smaller the 100-μm flux density is. (c) and (d): surface brightness profiles showing the effect of moving the fossil shell further or closer, through a variation of $T_1(\text{ext})$. (e): the physical parameters of the models.

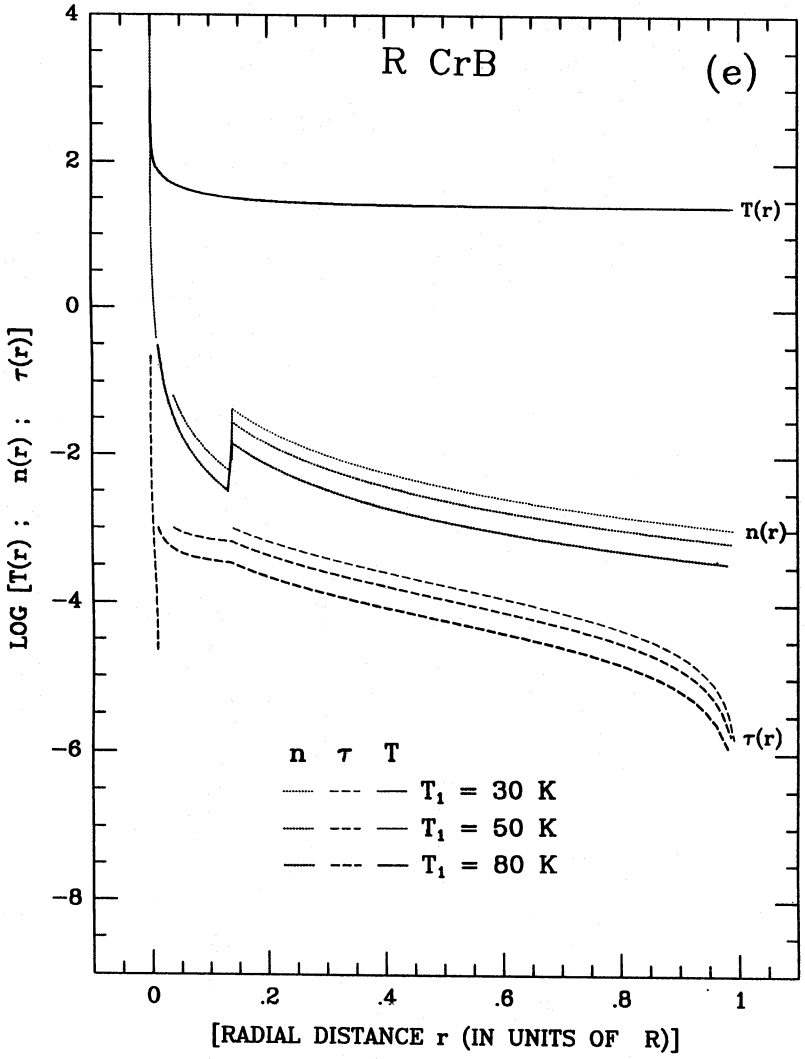

Figure 3 – *continued*

much from the $T_1(\text{ext}) = 50$ K case. The location of the extended shell actually represents the age of the remnant shell. The further the shell is from the central star, the higher its age. We conclude that the surface brightness of the fossil shell gradually increases as it moves away. The locations represented by $T_1(\text{ext}) < 50$ K are required for modelling the *IRAS* data of R CrB. We note that it is possible through high spatial resolution observations, to fix the radius at which the fossil shell begins.

2.3.3 *Effect of density exponent γ(ext) of the extended shell*

Fig. 4 shows a series of models using the RTM standard model, but for different values of the density exponent of the fossil shell: $\gamma(\text{ext}) = 1.5$, 1.9 and 2.3. Compared with the $\gamma(\text{ext}) = 1.9$ model, for smaller γ(ext) the amount of cool dust is large in the extended shell (particularly in the regions $p > 3$ arcmin), leading to increased emission at 60 μm and 100 μm. The reverse is true for larger γ(ext). The brightness fit for central positions depends indirectly on short-wavelength (≤ 30 μm) emission from the inner shell, rather than the physical properties of the extended shell. We find that, for closer positions [$T_1(\text{ext}) = 80$ K], a model with $\gamma(\text{ext}) \approx 1$ provides a better fit than the $\gamma(\text{ext}) = 1.9$ case. It is interesting to note that a single continuous shell model may also fit the R CrB data, with a 3–10 ISRF environment around the shell, if we employ $\gamma(\text{ext}) \approx 1$ (implying a variable rate of mass loss in a uniformly expanding shell). If $\gamma(\text{ext}) \approx 2$ is used instead (constant rate of mass loss with constant expansion velocity), we require a stronger external heating (10–30 ISRF). Finally, although increasing $\tau_{0.55\,\mu\text{m}}$(ext) has a similar effect as increasing the strength of external radiation, for regions $p > 2$ arcmin it leads to undesirable enhancement of intensity in the region $p < 2$ arcmin, caused by a larger concentration of dust grains near the inner boundary owing to a power law type density distribution.

We want to emphasize that the relative position of the remnant shell is an important parameter. It relates directly to the evolutionary models of AGB phase (Schönberner 1977). Unfortunately, our models which fit the *IRAS* data, cannot give the exact position of the fossil shell, since all other model parameters are not strongly constrained. Although we can fit the observed data with a model using a certain value for the location of the fossil shell, just a 20 per

cent variation in the density exponent γ(ext), and a small adjustment of opacity index m, can fit the *IRAS* data even for largely different locations such as r_1(ext) = 1.4, 0.4 and 0.12 arcmin. Whereas an uncertainty of this magnitude in γ(ext) is acceptable, such wide differences in the location of the fossil shell are not, as the latter are connected closely with the evolutionary status of R CrB and the nature of mass loss. The density exponent essentially describes the type of mass loss in the dust wind. Since steady mass loss with a constant velocity of expansion is conventionally used

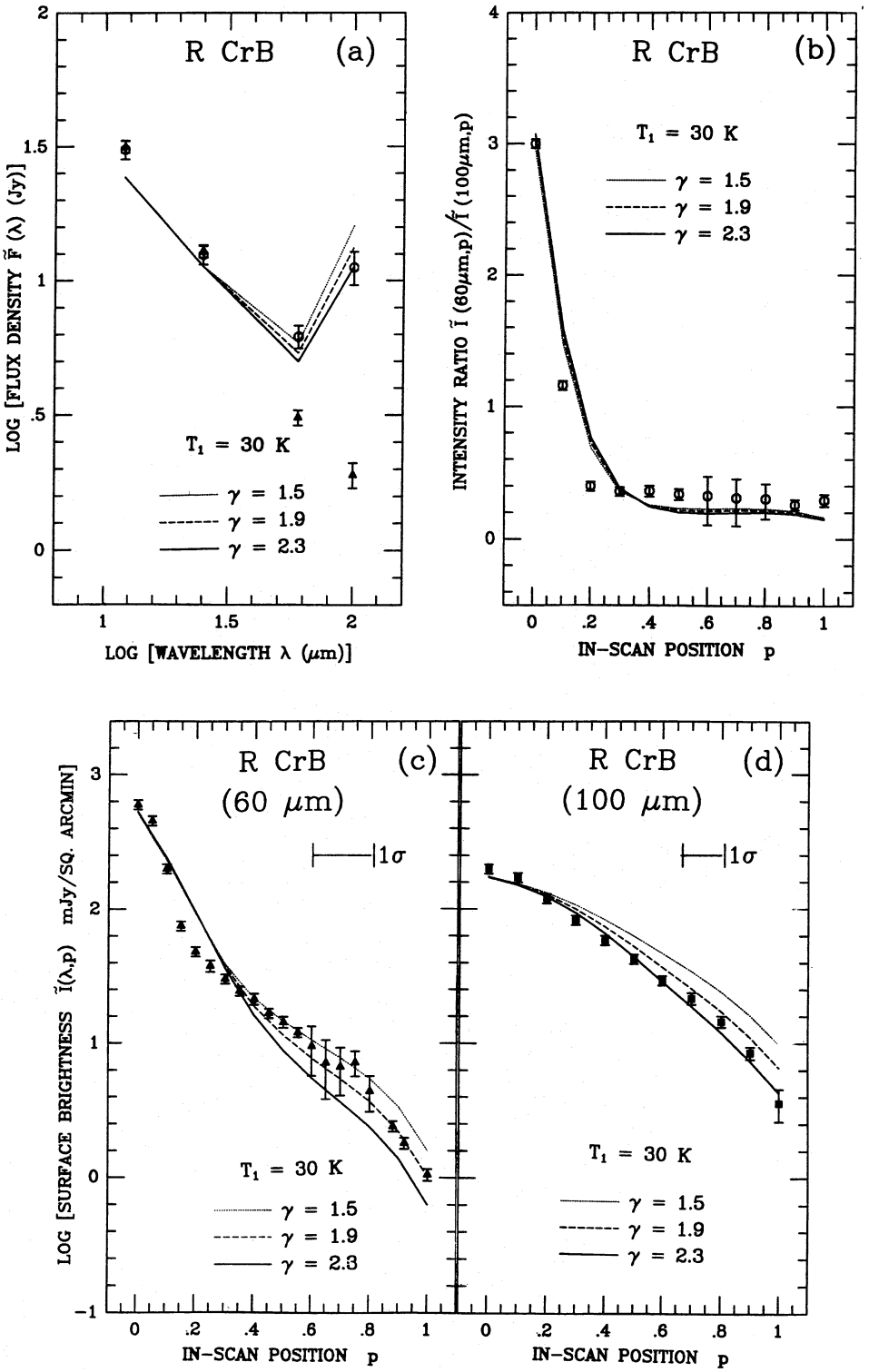

Figure 4. The effect of variation of the density exponent γ(ext). The position of the shell is r_1(ext) ≅ 1.4 arcmin corresponding to T_1(ext) = 30 K. (c) and (d): surface brightness profiles for this distant location of the fossil shell provides a good fit. The case with γ(ext) = 1.9 represents a common link with other figures. (e): physical parameters of the models.

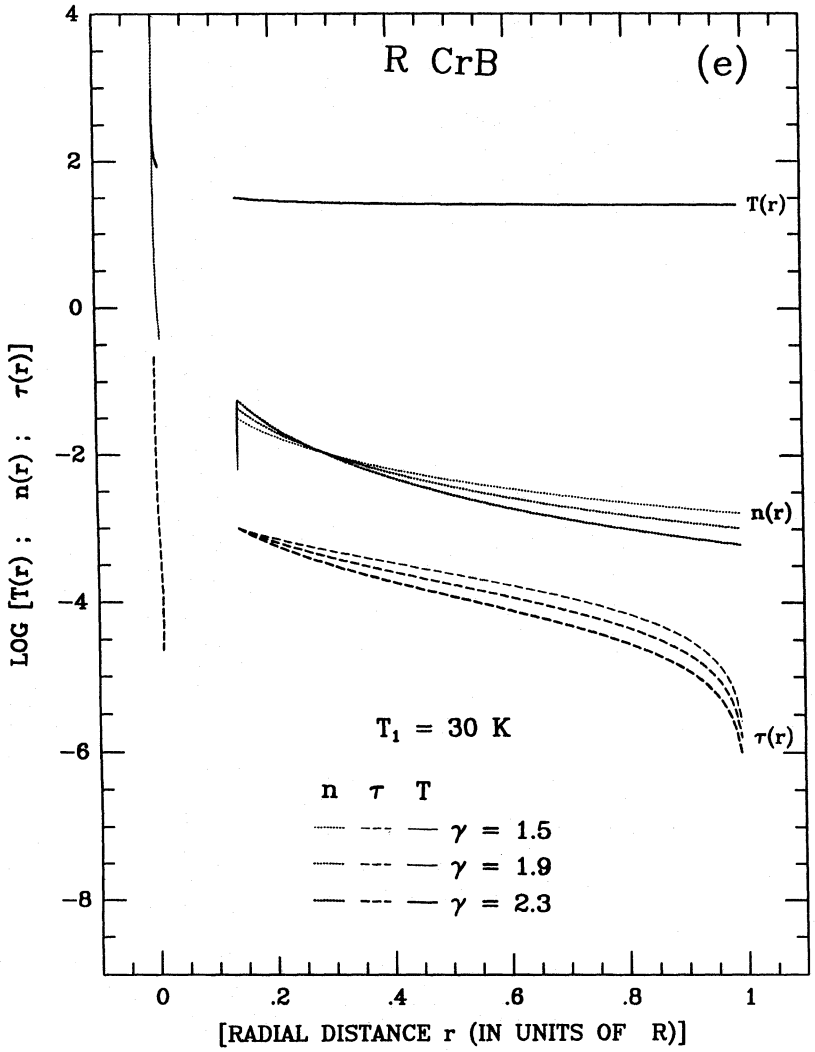

Figure 4 – *continued*

by several authors, we have preferred values of $\gamma(\text{ext}) \simeq 2$ as standard. Fig. 4 illustrates the changes in brightness profile when the mass loss changes from steady state, at a given epoch, or during the evolution of the system. Through narrow spectral band and high spatial resolution observations, it is possible to measure the spatial density variation of dust in the fossil shell. We conclude that $\gamma \sim 2$ is a reasonable choice for modelling the *IRAS* data.

2.3.4 *Effect of ISRF on extended shell temperature structure*

In Fig. 5 we show the effect of ISRF on the flux density and brightness profiles when the extended shell is situated in a position corresponding to $T_1(\text{ext}) = 30$ K. Once again the RTM standard model is employed. Although the external radiation used is very strong [large values of $C(\text{ext})$], it is not adequate to heat the dust to temperatures greater than 100 K in the extended shell, so that fluxes at wavelengths shorter than 30 μm are not affected. Keeping all other parameters constant, an increase in ISRF increases only the fluxes longward of 30 μm. The intensity ratio for $p > 3$ arcmin also shows a similar behaviour: the stronger the ISRF is, the larger is this ratio. However, for $p < 3$ arcmin, a reversal of this behaviour is seen, since the 60-μm brightness increases much more slowly, compared with the 100-μm brightness, which increases linearly as the ISRF is increased. The contribution of radiation from the inner shell to the 60-μm emission is significant in this part of the ext shell. Secondly, the ISRF spectrum itself has a sharp bump longward of 60 μm, and it penetrates easily into the $p < 3$ arcmin region. For closer positions [$T_1(\text{ext}) = 50, 80$ K] of the fossil shell, heating from stellar radiation naturally dominates over that of ISRF. It is clear that outer parts of the extended shell cannot be maintained at an equilibrium temperature of $\simeq 30$ K, unless heating by an external radiation field is invoked. We conclude that strong ISRF environment is inevitable in modelling the *IRAS* data of R CrB in order to explain the observed isothermal structure of the extended shell.

2.3.5 *Effect of total optical depth $\tau_{0.55\,\mu m}$(ext) of the extended shell*

In Fig. 6 we show how total optical depth affects the transfer of radiation field in the fossil shell. We have employed the RTM standard model for this series of models. Since we use a [γ(ext) = 1.9] power law density distribution in these models, changing $\tau_{0.55\,\mu m}$(ext) basically changes the dust density at all positions in the shell. The intensity ratio remains constant, independent of the optical depth in the

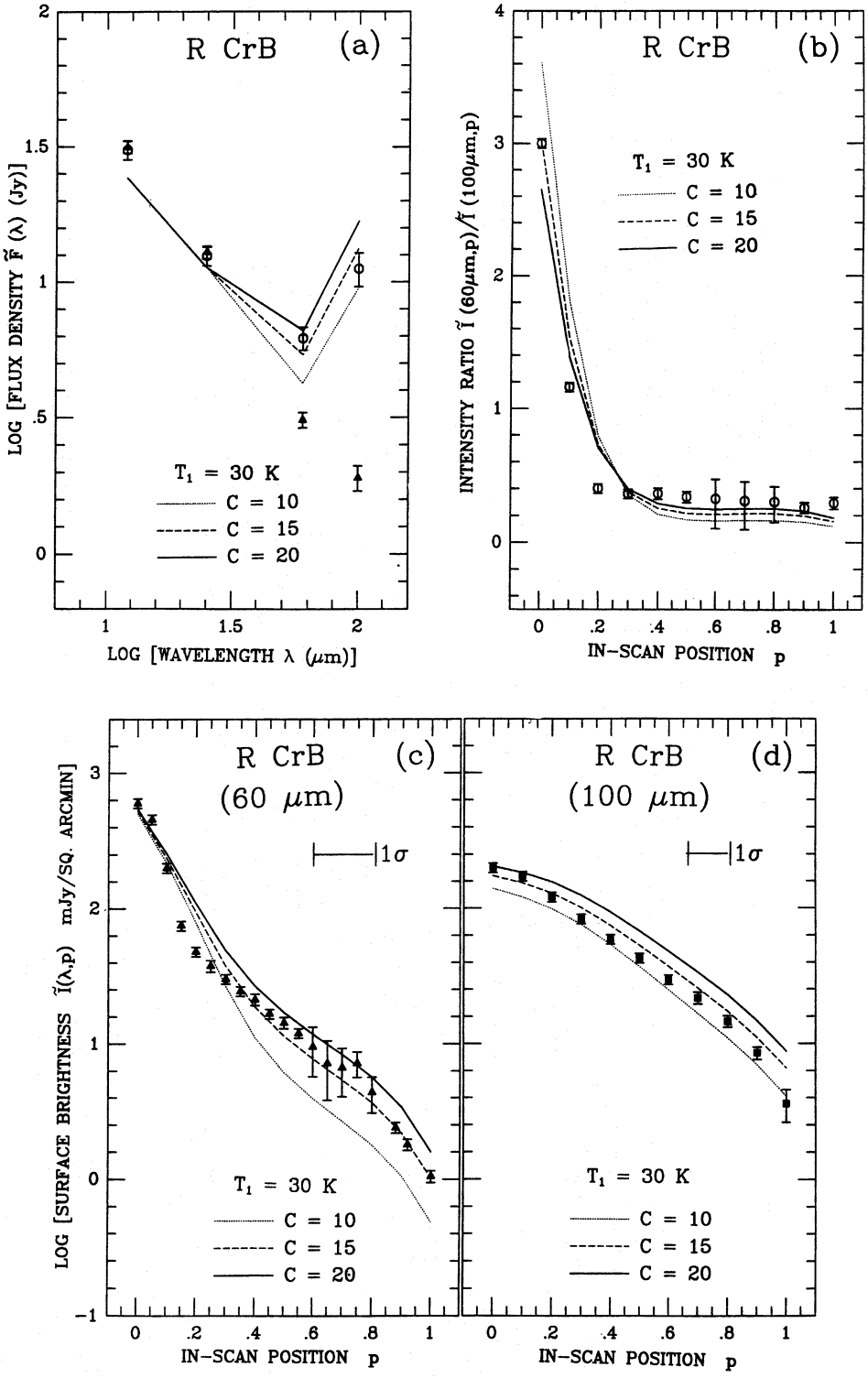

Figure 5. The effect of changing the strength of incident ISRF in radiative transfer models. C(ext) is the free parameter. T_1(ext) = 30 K. See Fig. 6 also for a similar behaviour.

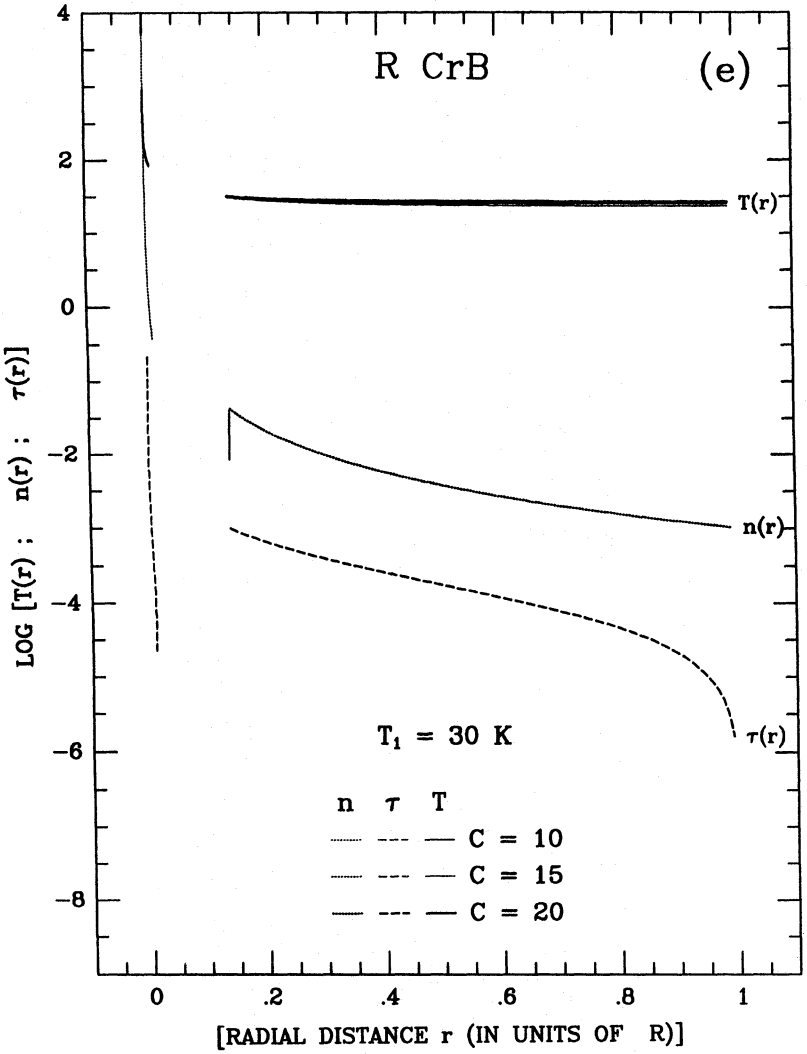

Figure 5 – *continued*

outer part of the shell. However, in the inner regions, the intensity ratio decreases as the optical depth increases, owing to a slower increase of the 60-μm brightness for $p < 3$ arcmin compared with the linear increase of the 100-μm brightness with optical depth. The optical depth effect is significant near the inner boundary of the fossil shell, as a large contribution to $\tau_{0.55\,\mu m}$(ext) comes essentially from these parts of the shell. The increase of emission with optical depth is linear for $p > 3$ arcmin, because the extended shell is genuinely optically thin in the far-infrared. If the optical depth is large or the dust scattering dominates (high albedo), then the above conclusion does not hold. The dust particles efficiently absorb optical and UV photons and emit thermal radiation almost entirely at long wavelengths. Thus the mechanism characterizing the local dust temperature is non-local in nature. When photons at short wavelengths are absorbed and subsequently emitted at longer wavelengths, the emitted photons travel greater distances in the dusty atmosphere because the photon mean free path $l(\lambda) \approx [\kappa(\lambda)]^{-1}$ increases. This random walk leads to coupling of different geometrical positions characterized also by dust particles of different temperatures. The situation is analogous to the transfer of spectral-line radiation in the wings of a scattering-dominated line. This characteristic of transfer of radiation in a dust cloud, coupled with the usual peculiarities of radiative transfer in spherical geometry (see Nagendra 1988), make even a simple problem of transfer of continuum radiation in an absorbing dust cloud hard to interpret. Although optical depth is an integrated quantity, it includes the basic nature of dust particles and their spatial distribution, and is better suited for RTM as an independent variable. We conclude that $\tau_{0.55\,\mu m} = 10^{-3}$ in the standard RTM model setup is reasonable for R CrB fossil shell.

The nature of the dust in RCB stars constitutes an important question. There is sufficient observational data regarding this point: the UV extinction curve for RY Sgr has a peak in the 2400–2500 Å range, which can be fitted well by pure amorphous carbon dust (Holm, Wu & Doherty 1982; Hecht et al. 1984; Wright 1989; Hecht 1991). Since then several studies have confirmed and extended this result. Hecht at al. (1984) found that the dust extinction curves measured during minima of R CrB and RY Sgr are consistent with extinction from glassy or amorphous carbon grains

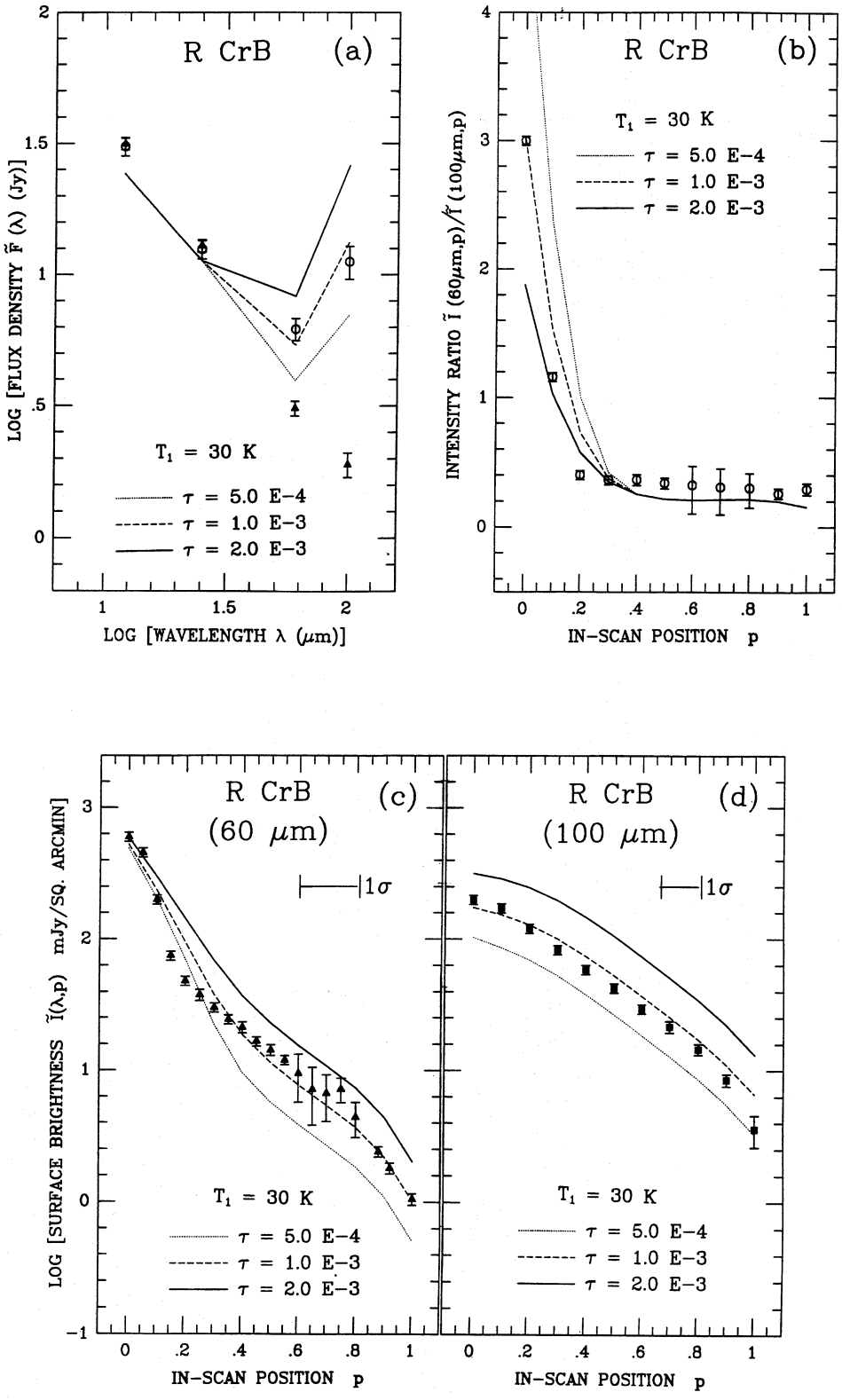

Figure 6. The effect of varying the total optical depth $\tau_{0.55\,\mu m}$ (ext) on the R CrB model results. T_1 (ext) = 30 K. Since the fossil shell is optically thin in the layers corresponding to $p > 3$ arcmin, the brightness variation is linear in both bands: larger $\tau_{0.55\,\mu m}$ (ext) leads to a stronger 60- and 100-μm brightness.

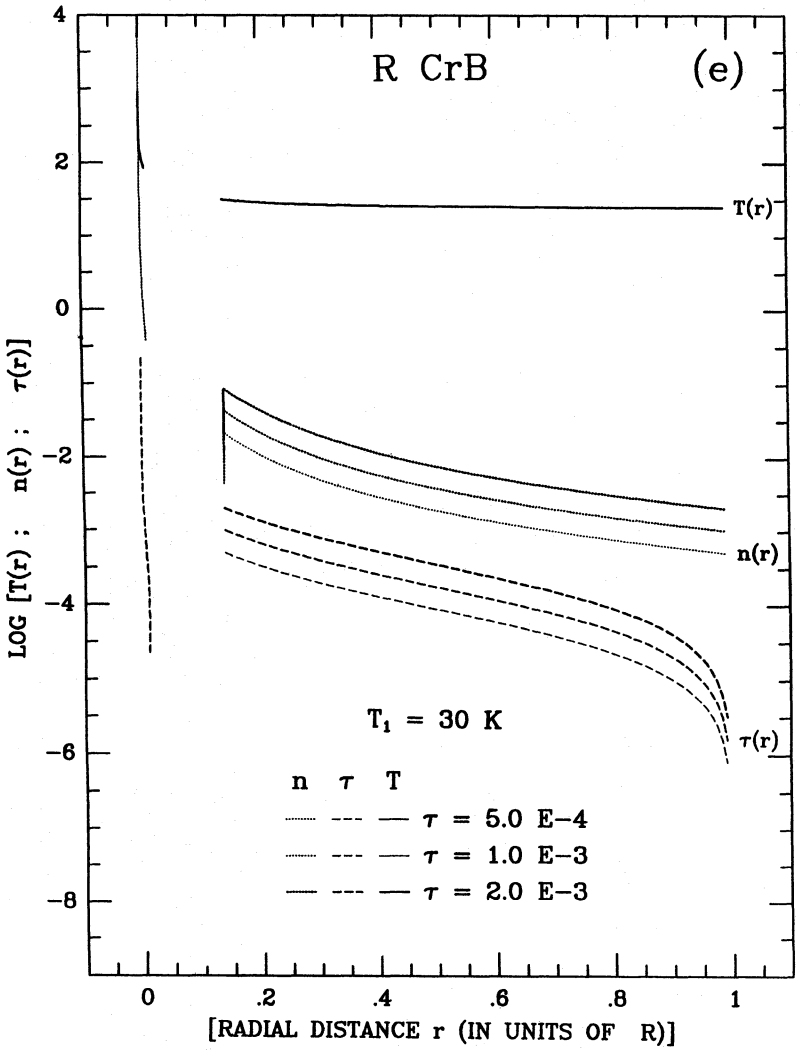

Figure 6 – *continued*

with a size distribution in the range 0.005–0.06 μm. Similar extinction curves have been found for RY Sgr (Clayton et al. 1992); R CrB (Holm et al. 1987; Holm & Doherty 1988); V348 Sgr (Drilling & Schönberner 1989) and MV Sgr (Evans et al. 1985). Recently, Jeffrey (1995) considered the UV extinction properties of other carbon materials such as fullerenes in several H-deficient and C-rich stars.

2.3.6 *Effect of density contrast in the [r_1(ext), R] region of the extended shell*

RTM standard models are employed in this series of runs also, except that C_2(ext) is a free parameter. In all our models of R CrB, it is necessary to employ a density enhancement starting at the reference radius r_1(ext) = 1.4 arcmin irrespective of where the extended shell is actually located. By density enhancement, we mean an increase of dust density over and above that given by the same power law applied to both the compact and the fossil shells. This is equivalent to accumulation of cold dust as a result of some mechanism. A possible explanation could be a drop in the velocity of new dust wind at this radius, because of collision with a pre-existing fossil shell having a larger but constant mass-loss rate. Such a density contrast has also been employed in the optically thin models of Gillett et al. (1986). We find that the density enhancement is equivalent to the presence of large sized grains in the colder [T(ext, r) < 30 K] extended layers. Fig. 7 shows this effect for a location of the ext shell, represented by T_1(ext) = 30 K. The amount of cold dust and optical path length (in the extended shell) for all the lines of sight is larger with respect to this location of the fossil shell, compared to a closer location [say T_1(ext) = 80 K] of the ext shell. As the dust concentration is increased [C_2(ext) ≠ 1], the 12- and 25-μm fluxes decrease, because of absorption by cold dust [T(ext, r) < 30 K] which emits only at long wavelengths. The 60- and 100-μm fluxes are not much affected, however, because of a strong saturating influence of ISRF in these layers. For locations close to the inner shell, the density enhancement at r_1(ext) = 1.4 arcmin, on the other hand, leads to a stronger influence on brightness profiles. It is primarily because the density contrasted layers of dust (starting always at p > 1.4 arcmin) intercept 60- and 100-μm radiation emitted from the inner shell, which is not yet geometrically diluted. The 60- and

100-μm extended emission does not depend linearly on the enhancement of C_2(ext): a saturation of brightness is reached for [C_2(ext) > 10]. We conclude that [C_2(ext) ~ 1–5] is a reasonable choice for modelling the *IRAS* data. Since the mass-loss rate of R CrB is rather small, it appears that more than one episodic event may have occurred in the past to enhance the dust density in the fossil shell. An observational consequence of such accumulation is a local spike in brightness near the inner edge of the fossil shell for short-wavelength radiation – although high spatial resolution would be required in order to overcome beam-averaging effects and detect such a spike.

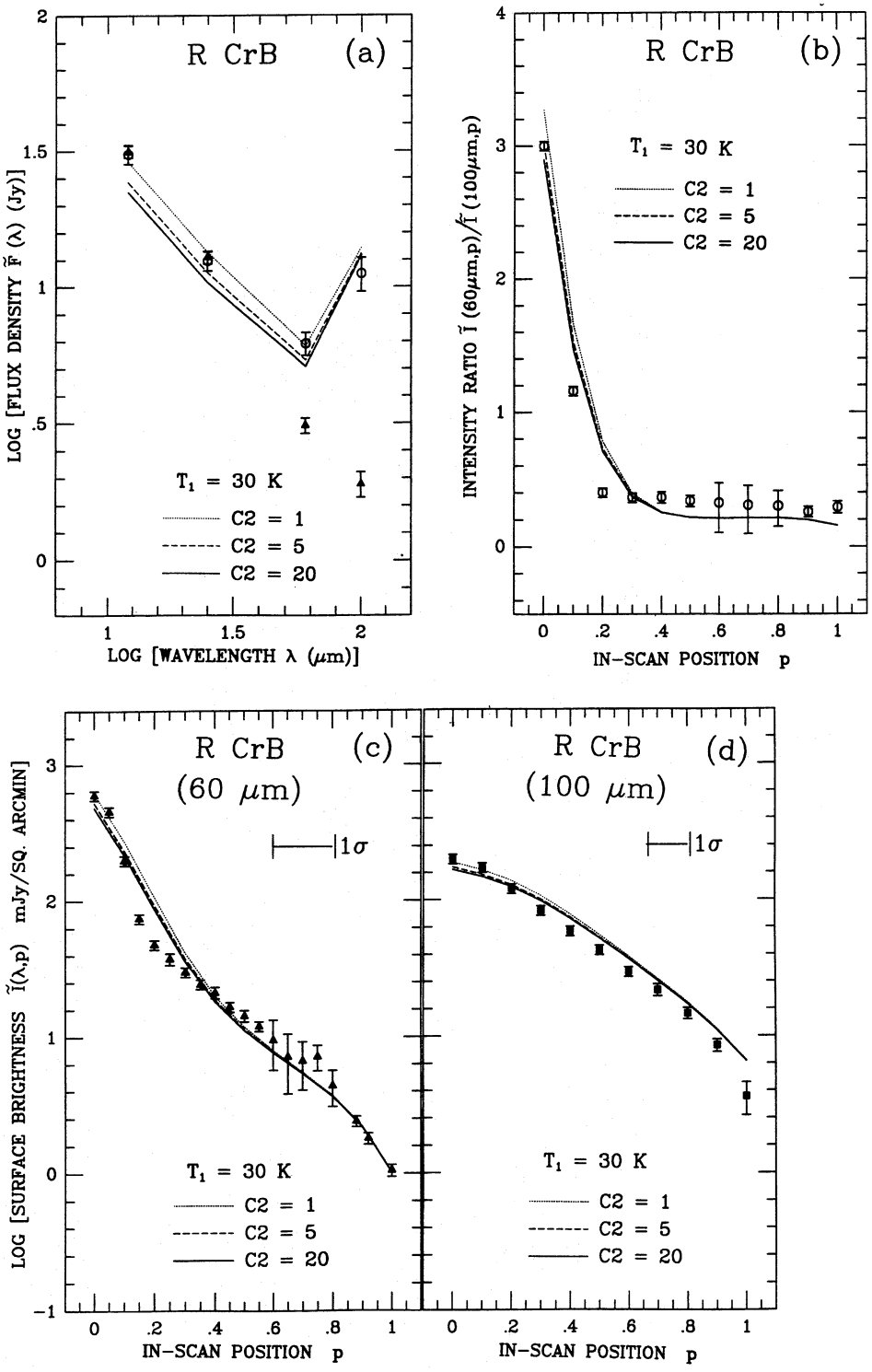

Figure 7. The effect of changing the density contrast parameter C_2(ext) of the fossil shell. The density enhancement occurs only for $p > 1.4$ arcmin. The flux densities in 12- and 25-μm are significantly affected because of obscuration by cold dust. However, this factor C_2(ext) has only a minor effect on the brightness profiles except near the inner edge.

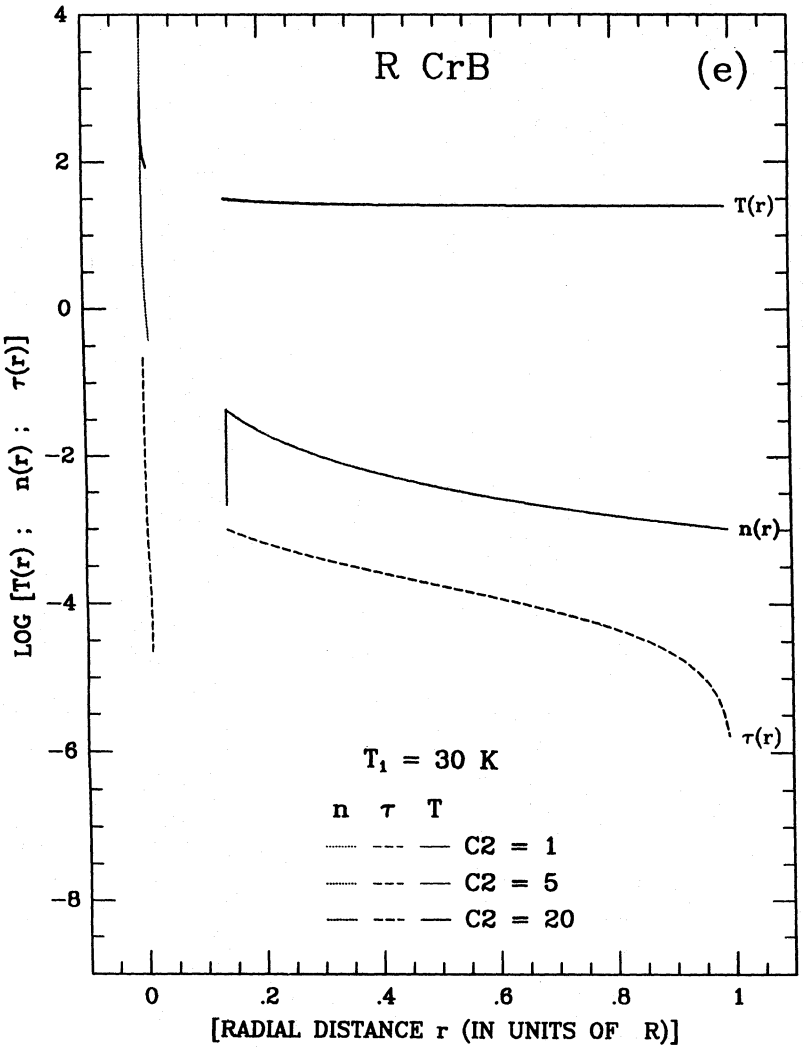

Figure 7 – *continued*

2.4 Some general remarks on our modelling approach to *IRAS* data

In our RTM models of R CrB, only when the dust temperature in the extended shell is nearly constant in the range 30–25 K do we get qualitative fits to the data. To maintain this near constancy of $T(\text{ext}, r)$ across such a large shell, we require a very strong ISRF now [namely through the factor $C(\text{ext}) = 10\text{–}30$]. Since the results depend sensitively on various physical and geometrical parameters of both shells, we select the set of parameters which approximately fit the data (the RTM standard model), and then vary the free parameter in question around a median value. In this manner, the effect of varying a single parameter in question on the two-component model can be understood. In all the RTM models of R CrB presented in this paper, the characteristics of a compact shell are fixed, and only the parameters of the extended shell (ext) are varied. The AM approach gives fairly accurate results when the condition $\tau_{uv}(r) \ll 1$ is genuinely satisfied for all the depth points, where $\tau_{uv}(r)$ is the optical depth scale in the uv region of the spectrum. Errors arise in the computation of fluxes and the temperature structure $T(r)$ for moderate values of optical thickness, due to the neglecting of radiative transfer effects. This problem is particularly acute if the dust opacity is scattering dominated. However, for optically very thick media the radiation field saturates to local thermal equilibrium values through most of the shell, and at least a simple LTE (local thermodynamic equilibrium) transfer approach instead of AM becomes necessary.

2.4.1 *Effect of beam dilution on long-wavelength surface brightness*

Here again, we employed RTM standard models. To study the effect of beam sizes on the computed surface brightness profiles, we use Gaussian beams of projected half widths $r_{b,100\,\mu m} = 2.25$ arcmin and $r_{b,60\,\mu m} = 1.25$ arcmin at the source. They give approximately the same beam areas as the (3 × 5 arcmin) and (1.5 × 5 arcmin) rectangular beams of *IRAS* detectors. We find that the difference in result between a uniform beam and a Gaussian beam is $< 1\text{–}10$ per cent, depending on beam position on the disc. This choice of beam sizes gives a 'disc-integrated flux' (obtained by inte-

grating on the 'beam-convolved mean brightness' computed at several positions p on the visible disc), which is accurate to ± 5 per cent of the observed fluxes. In Fig. 8 we show the effect of performing beam convolution using different beam sizes for the model with $T_1(\mathrm{ext}) = 50$ K. The three cases correspond to Gaussian beam diameters $2r_{\mathrm{b},100\,\mu\mathrm{m}} = (4.05$ arcmin; 4.5 arcmin; 4.95 arcmin) and $2r_{\mathrm{b},60\,\mu\mathrm{m}} = (2.25$ arcmin; 2.5 arcmin; 2.75 arcmin) respectively. This choice represents a ± 10 per cent variation around the median beam sizes employed throughout this paper. Notice that the results

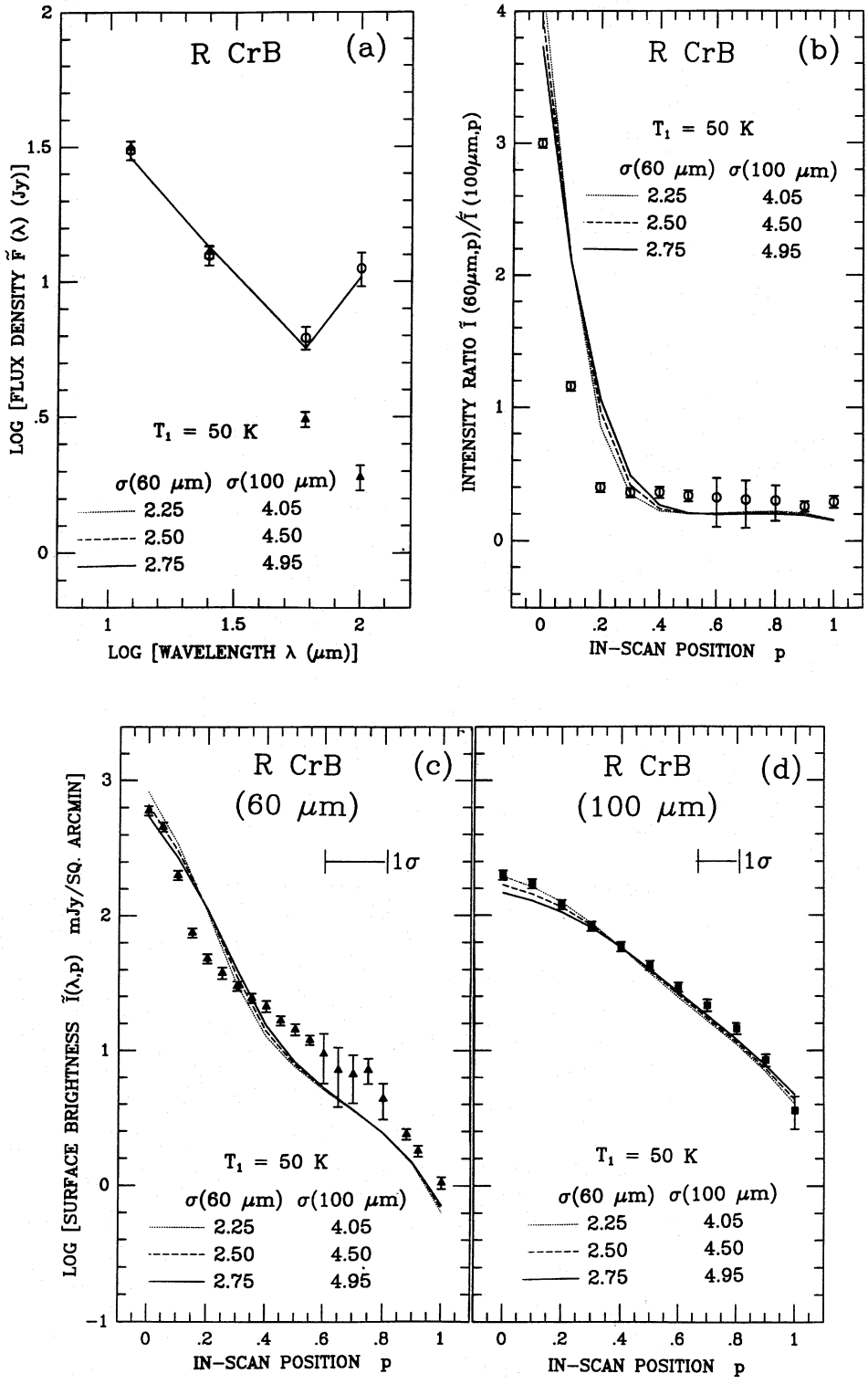

Figure 8. The effect of beam size on model results for the location $T_1(\mathrm{ext}) = 50$ K of the fossil shell. The three cases correspond to a variation of 10 per cent about the standard beam sizes $r_{\mathrm{b},100\,\mu\mathrm{m}} = 2.25$ arcmin and $r_{\mathrm{b},60\,\mu\mathrm{m}} = 1.25$ arcmin employed throughout this paper. The beam size variation can significantly affect the surface brightness profiles and the intensity ratio.

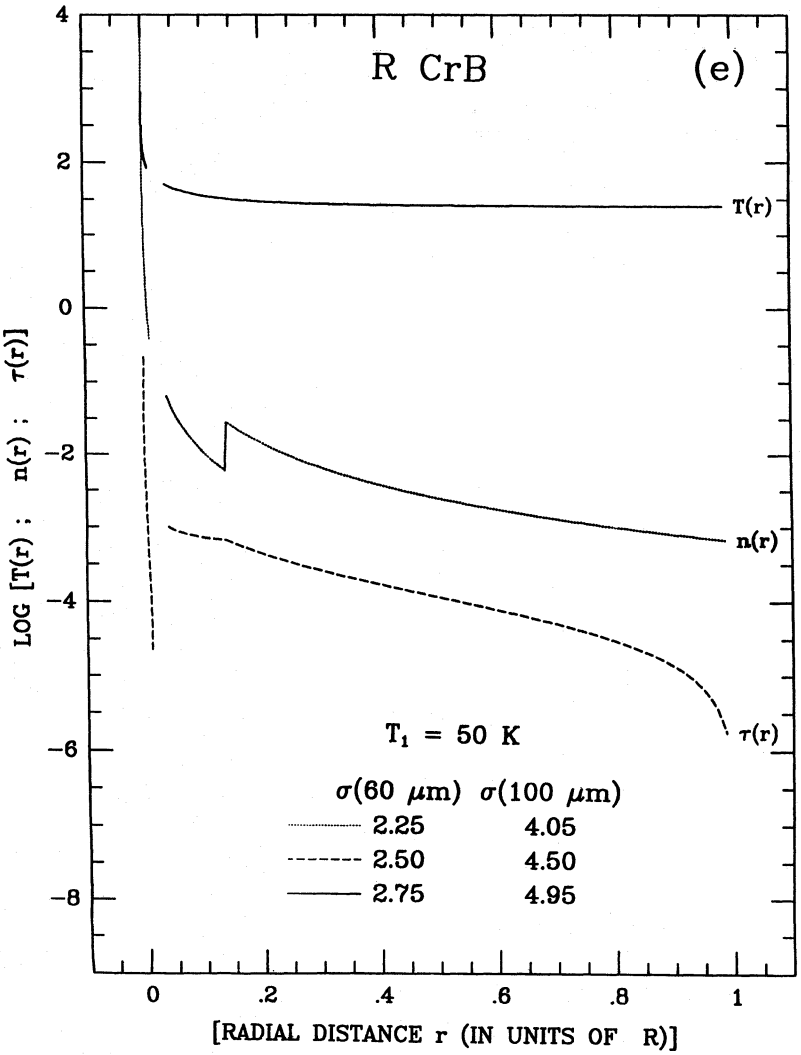

Figure 8 – *continued*

differ only by a few per cent at the limb, and to a maximum of 15 per cent at the disc centre. To handle the strong variation of specific intensity $I(\lambda, P)$ with frequency and position, we use 340 non-uniformly placed radial grid points (340 lines of sight) in solving the transfer equation. This provides a good original P-grid resolution [see equation (A6)], which is needed to perform accurate spatial convolution integration. We also employ a very fine r grid that depends on beam position p on the disc and on the scan angle θ measured in the two-dimensional beam coordinate system. For single shell models however, a smaller number of points (100 to 50 points) in P grid are sufficient. We conclude that appropriate beam pattern and accurate beam convolution on theoretical intrinsic profiles should form a basic part of modelling the surface brightness data.

2.4.2 *Non-uniqueness of the IRAS flux spectrum modelling*

To emphasize the need for using both the surface brightness and flux density in fitting the *IRAS* data, we present a set of three models designated as Models 1–3 (dotted, dashed and full lines respectively) in Figs 9(a)–(e). In Table 2 we list some of the best fitting input parameters. The models are computed in the same way as discussed in Section 2.3. From Table 2, we see that the sets of input model parameters are very different from each other. However, as shown in Fig. 9(a), all these models approximately fit the observed flux-density data. Indeed Model 1 (dotted line) and Model 2 (dashed line) give nearly identical fluxes. The intensity ratio, however, is different in Models 1 and 2. Nevertheless, all three models appear to fit the intensity ratio in the region $p > 3$ arcmin fairly well (Fig. 9b). It is only the individual surface brightness fits in Figs 9(c)–(d) which help eliminate Model 1 and Model 3 as less suitable. Model 2, with small improvements, can be one of the better models since it fits the flux density, intensity ratio, and surface brightness data simultaneously. Thus if the constraint of observed surface brightness is not utilized, it is hard to narrow down the range of physical parameters. For illustration, some parameters derived from these three models are shown in Table 3.

2.4.3 *The limitations of our modelling approach*

We have tried to show the physical effects of various parameters involved in circumstellar double- or multi-shell modelling. Since there are many independent variables, the ranges of which are unknown by any independent means, it is difficult to model the surface brightness data purely by the RTM approach. It is advisable to perform fast trial-and-error modelling by employing only the AM approach. We hope that this method works at least for R CrB and other optic-

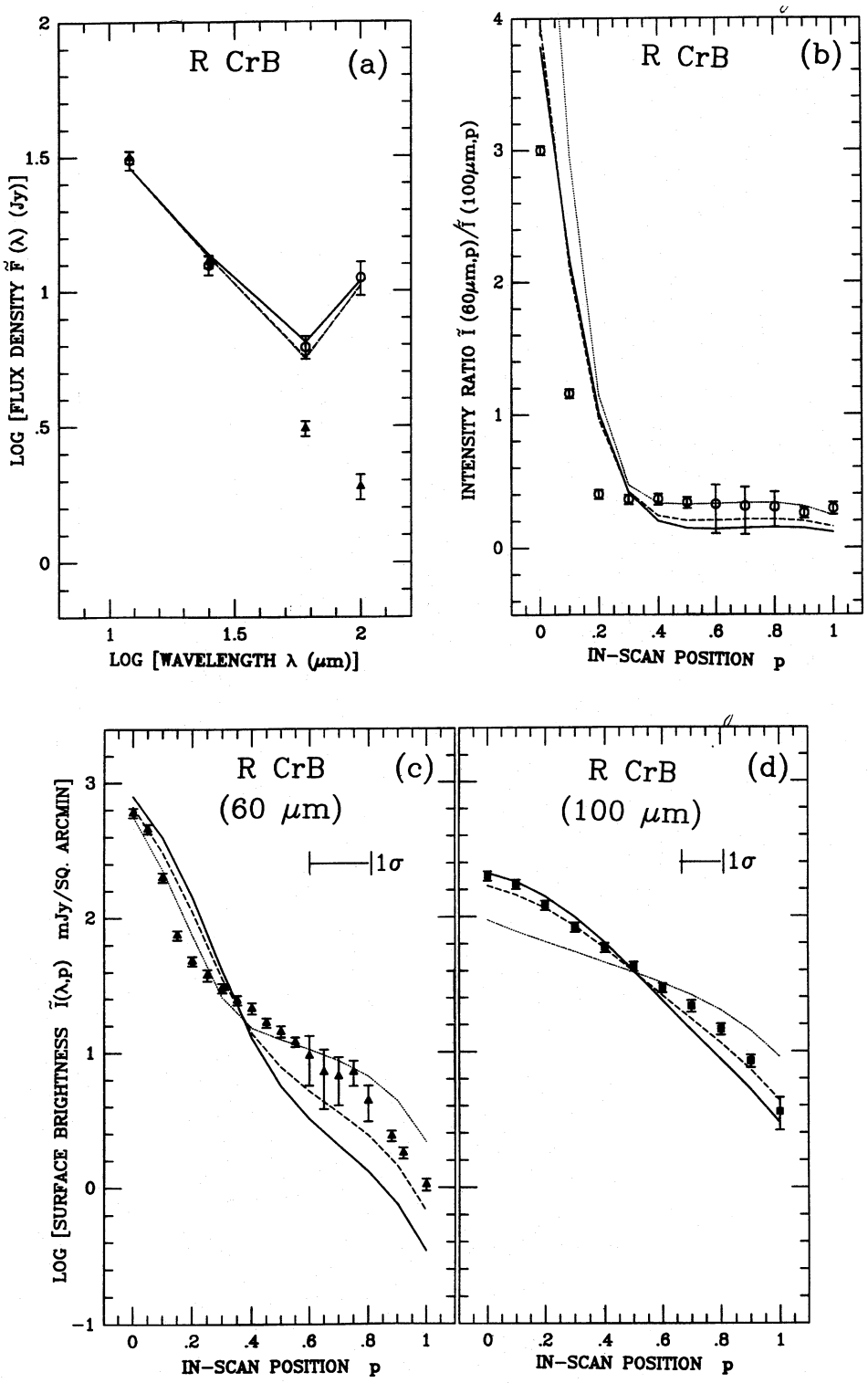

Figure 9. Miscellaneous models of R CrB. Models shown here demonstrate the need to fit *IRAS* flux density and the surface brightness simultaneously. Some input parameters for these models are given in Table 2. The rest of the parameters are same as the standard model set (see Section 2.1). The derived parameters are given in Table 3.

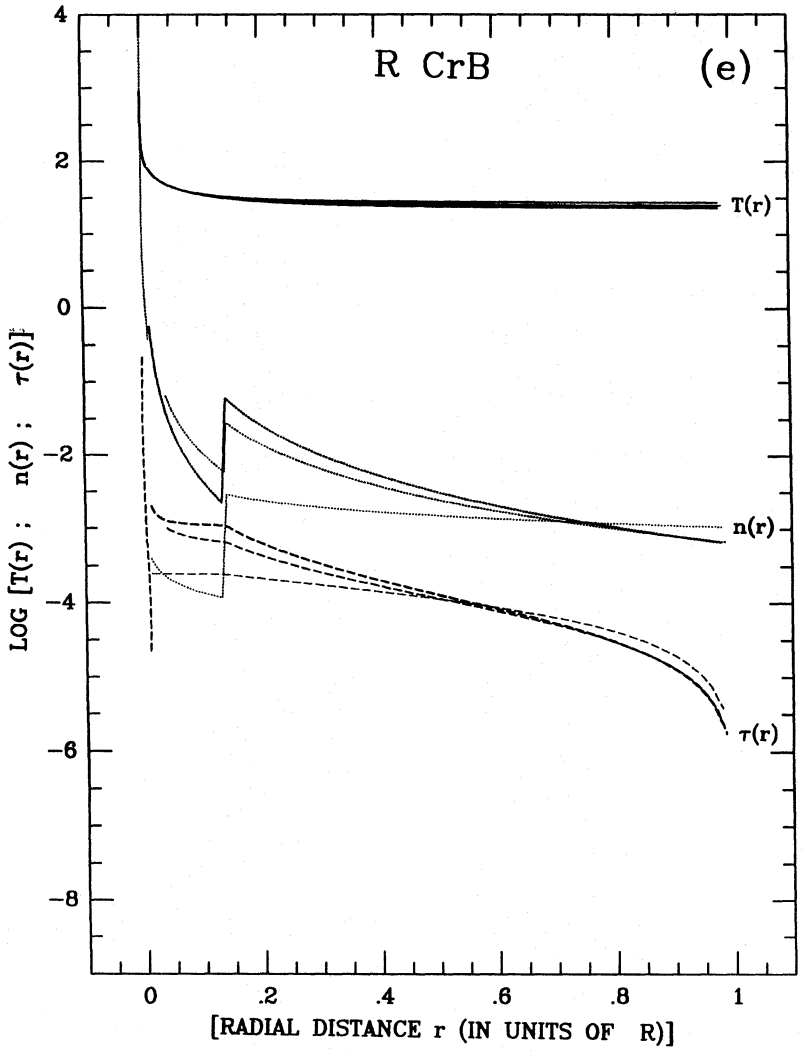

Figure 9 – *continued*

Table 2. Some input parameters for models shown in Fig. 9.

Parameter	Model 1	Model 2	Model 3
$T_1(ext)$ (K)	80	50	80
$\gamma(ext)$	0.5	1.9	2.3
$C(ext)$	25	15	10
$C_2(ext)$	25	05	30
$\tau_{0.55\ \mu m}(ext)$	$2.5\ 10^{-4}$	$1.0\ 10^{-3}$	$2.0\ 10^{-3}$

Table 3. Some quantities derived from model fits shown in Fig. 9.

Quantity	Model 1	Model 2	Model 3
$T(ext, 3')$ (K)	29.4	27.3	26.0
$\tau_{0.55\ \mu m}(ext, 3')$	$1.8\ 10^{-4}$	$2.6\ 10^{-4}$	$3.4\ 10^{-4}$
$\dot{M}_d(ext, 3')$ $(M_\odot/yr)$	$2.4\ 10^{-9}$	$8.1\ 10^{-9}$	$1.3\ 10^{-8}$
$M_d(ext)$ $(M_\odot)$	$2.5\ 10^{-4}$	$7.4\ 10^{-4}$	$9.1\ 10^{-4}$

ally thin circumstellar shells. For optically thick shells, we need to employ the RTM approach even for trial and error.

The main limitations of our semi-quantitative study are the use of power law opacity and power law space density distributions in the dust shells, apart from using uniform dust particle radius. Relaxing one or all of these three assumptions may provide improved models of R CrB dust shells. The power law density distribution can be replaced by a linear combination of several power laws or any other physically reasonable distibution. For instance, some of our models, not discussed in this paper, show that a Gaussian density distribution (instead of a power law) in a small ($r \approx 1$ arcsec diameter) core region can improve the fit to brightness data in the $p < 3$ arcmin region. This, however, intro-

duces one or more free parameters to the problem, which is not advisable. Also, it is clear that models of fossil shells cannot be constructed only based on *IRAS* data at four wavelengths. An integrated approach at modelling the flux density and surface brightness at wavelengths shorter than 12 μm, and longer than 100 μm (submm range) is necessary to make systematic progress.

3 IMPLICATIONS AND CONCLUSIONS

Our radiative transfer models are computed by a self-consistent solution of the radiative transfer and energy balance equations in spherical geometry. Using these models to fit the *IRAS* data for R CrB, we find that our models require a considerable detachment of fossil shell from the inner hot shell to fit the observed data.

We conclude that the identification of an extended shell in R CrB as a fossil shell by Gillett et al. (1986) is essentially correct. A constant but considerably larger episodic mass-loss rate in this fossil shell, seems appropriate compared to that required in the conventionally used single-shell scenario. High values of ISRF are necessary to fit the *IRAS* data if we are to retain the picture of constant, although different, mass-loss rates with the same velocity of expansion, for both shells. The extended shell may have density distributions with power-law indices in the range $\gamma(\text{ext}) \approx 1.0$–$1.5$ as alternatives, but they represent a quite different set of models.

The ISRF required for RTM is larger than suggested by the optically thin models of Gillett et al. (1986). It appears that only ISRF heating is effective in establishing a constant dust temperature in a detached shell. Although it is difficult to identify another mechanism which produces this isothermal structure of the fossil shell, local impulsive heating of very small grains by central star radiation, which subsequently emit strongly at 12 and 25 μm, is a possibility (Feast 1990). The small grains can affect the 60-μm surface brightness and the 60- to 100-μm intensity ratio in the inner parts of the extended shell, and help also to improve the model fits in that region. There is no difficulty, however, in modelling the 100-μm surface brightness arising in the outer layers by employing the usual large grains model (meaning, the standard RTM model with grain radius in the range 0.01–0.05 μm). The heating of large grains in the outermost layers by regular ISRF is still a reasonable assumption. The grains are more likely to be amorphous carbon or carbon-based grains in the R CrB fossil shell. Other conclusions from our models are as follows.

(1) Our two-shell model for R CrB can be applied to model other similar sources. One can choose two entirely different sets of physical parameters for the inner hot shell, and the extended fossil shell. The crucial parameter is the distance of separation between the fossil shell and the hot inner shell.

(2) Our procedure of modelling the integrated flux density data and the unprocessed surface brightness data in the *IRAS* bands, using a single set of model parameters for the whole system (central star, inner hot dust shell and cold detached fossil shell taken together) seems to be correct. It is equivalent to the modelling of 'point-source processed flux' and 'point-source response deconvolved brightness', as is done in earlier studies of R CrB.

(3) No single power law density distribution can fit the *IRAS* surface brightness data (in both the 60- and 100-μm bands) of R CrB across the entire source. The density distributions near the inner boundaries of the hot shell, as well as the extended shell are certainly of a composite power-law type.

(4) Except for the self-consistent determination of the temperature structure, no greater insights are obtained from the radiative transfer modelling alone, when the circumstellar dust shells are optically thin. It is rather useful to construct full analytic models (as we have done in this paper) as preprocessors to the more involved transfer calculations. The analytical models help us narrow down easily the range of free parameters.

ACKNOWLEDGMENTS

KNN is grateful to IAU Commission 38 for a travel grant. The entire work on this paper was performed when he was visiting the Department of Physics, Applied Physics and Astronomy, RPI, Troy, New York. He would also like to thank Michael Egan, Steven Doty and Don Mizuno for their help, and Darek Lis and Steven Charnley for useful comments. This work has been partially supported by the U.S. Air Force under grant AFOSR 89-0104, and by the NASA grants NAGW-2817 and NAGW-3144. We are grateful to the referee Dr. Geoffrey C. Clayton for useful comments which helped in improving the paper.

REFERENCES

Clayton G. C., 1996, PASP, in press
Clayton G. C., Whitney B. A., Stanford S. A., Drilling J. S., 1992, ApJ, 397, 652
Clayton G. C., Kelly D. M., Lacy J. H., Little-Marenin I. R., Feldman P. A., Bernath P. F., 1995, AJ, 109, 2096
Doty S. D., Leung C. M., 1994, ApJ, 424, 729
Drilling J. S., Schönberner D., 1989, ApJ, 343, L45
Egan M. P., Leung C. M., Spagna Jr. G. F., 1988, Comput. Phys. Commun., 48, 271
Evans A., Whittet D. C. B., Davies J. K., Kilkenny D., Bode M. F., 1985, MNRAS, 217, 767
Feast M. W., 1975, in Sherwood V. E., Plaut L., eds, IAU Symp. No. 67, Variable Stars and Stellar Evolution. Reidel, Dordrecht, p. 129
Feast M. W., 1986, in Hunger K., Schönberner D., Rao N. K., eds, IAU Colloq. No. 87, Hydrogen Deficient Stars and Related Objects. Reidel, Dordrecht, p. 151
Feast M. W., 1990, in Cacciari C., Clementini G., eds, ASP Conf. Ser. Vol. 11, Confrontation Between Stellar Pulsation and Evolution. Astron. Soc. Pac., San Francisco, p. 538
Forrest W. J., Gillett F. C., Stein W. A., 1972, ApJ, 178, L129
Gillett F. C., Backman D. E., Beichman C., Neugebauer G., 1986, ApJ, 310, 842
Hawkins G. W., Zuckerman B., 1991, ApJ, 374, 227
Hecht J. H., 1991, ApJ, 367, 635
Hecht J. H., Holm A. V., Donn B., Wu C. C., 1984, ApJ, 280, 228
Holm A. V., Doherty L. R., 1988, ApJ, 328, 726
Holm A. V., Wu C. C., Doherty L. R., 1982, PASP, 94, 548
Holm A. V., Hecht J. H., Wu C. C., Donn B., 1987, PASP, 99, 497
Jeffery C. S., 1995, A&A, 299, 135

Leung C. M., 1976, J. Quant. Spectrosc. Radiat. Transfer, 16, 559
Mathis J. S., Mezger P. G., Panagia N., 1983, A&A, 128, 212
Nagendra K. N., 1988, ApJ, 335, 269
Rao N. K., Nandy K., 1986, MNRAS, 222, 357
Rowan-Robinson M., 1982, MNRAS, 201, 281
Schönberner D., 1977, A&A, 57, 437
Soifer B. T. et al., 1986, ApJ, 304, 651
Sopka R. J., Hildebrand R., Jaffe D. T., Gatley I., Roellig T., Werner M., Jura M., Zuckerman B., 1985, ApJ, 294, 242
Stein W. A., Gaustad J. E., Gillett F. C., Knacke R. F., 1969, ApJ, 155, L3
Van der Veen W. E. C. J., Trams N. R., Waters L. B. F. M., 1993, A&A, 269, 231
Van der Veen W. E. C. J., Waters L. B. F. M., Trams N. R., Matthews H. E., 1994, A&A, 285, 551
Walker H. J., 1985, A&A, 152, 58
Whitney B. A., Clayton G. C., Schulte-Ladbeck R., Meade M. R., 1992, AJ, 103, 1652
Whitney B. A., Balm S. P., Clayton G. C., 1993, in Sasselov D. D., ed., ASP Conf. Ser. No. 45, Luminous High-Latitude Stars. Astron. Soc. Pac., San Francisco, p. 115
Wright E. L., 1989, ApJ, 346, L89
Young K., Phillips T. G., Knapp G. R., 1993a, ApJS, 86, 517
Young K., Phillips T. G., Knapp G. R., 1993b, ApJ, 409, 725

APPENDIX A: SPECTRAL AND SPATIAL CONVOLUTIONS TO MODEL *IRAS* SURFACE BRIGHTNESS DATA

In this appendix we give the expressions employed by us to perform convolutions shown above. Our spatial convolution procedure is slightly different from that of Gillett et al. (1986). Basically, they estimate a system point source response (PSR) function, and convolve it with the theoretical intrinsic model surface brightness profiles. However, we compute Gaussian or uniform beam response functions with equivalent circular cross-sections of the *IRAS* beam sizes. These response functions are then convolved with the intrinsic model surface brightness profiles.

The *IRAS* spectral bandpass filters are quite wide (widths of 8, 16, 60 and 75 μm which are centred approximately at 12, 25, 60 and 100 μm respectively). Therefore, to compare model results with *IRAS*-observed data, we need to perform a spectral convolution on the theoretical fluxes $F(\lambda)$, using an appropriate spectral response function. Likewise, we perform a combined spectral plus spatial convolution on the computed specific intensity distribution $I(\lambda, P)$ for an impact parameter P, which is computed by the AM or RTM approaches as the case may be. The spectral response functions of all the four *IRAS* bands have been tabulated in the *IRAS* supplementary catalogue. The flux density in the *IRAS* bands are measured using telescope beam sizes larger than the source size (called point source mode of observation). For R CrB, the *IRAS* flux densities are measured with a 24 arcmin diameter beam, while the source diameter is approximately 18–20 arcmin.

To resolve a source, a beam size much smaller than the source size should be used. In fact, the smaller the beam size, the better the resolution and information content. The *IRAS* beam sizes are reasonably smaller to allow good disc-resolved measurements to be made. The beam sizes at 60 and 100 μm are respectively (1.5×5 arcmin^2) and (3×5 arcmin^2), with the short axis parallel to the in-scan direction. The convolved brightness $\tilde{I}(\lambda, p)$, is measured by centring such small beams at several positions p (related to P through expression A6) across the visible disc. The 60-μm brightness of R CrB for instance is measured at 17 positions (p) of the telescope beam on the visible disc of the source. The expressions we give below for beam pattern assume a circular cross-section for the beam. The convolution integrals are given by

$$\tilde{F}(\lambda_i)=\int_{A_{\lambda_i}}^{B_{\lambda_i}} G(\lambda_i, \lambda)F(\lambda)\,\mathrm{d}\lambda, \qquad i=1\text{–}4, \tag{A1}$$

for spectral convolution with the flux density, and

$$\tilde{I}(\lambda_i, p)=\int_{A_{\lambda_i}}^{B_{\lambda_i}} G(\lambda_i, \lambda)I^c(\lambda, p)\,\mathrm{d}\lambda, \qquad i=1\text{–}4, \tag{A2}$$

for a spectral + spatial convolution on the intrinsic intensity profile, where

$$I^c(\lambda, p)=\int_0^{2\pi}\mathrm{d}\theta\int_0^{\infty} S(\lambda, r, \theta)[I(\lambda, r, \theta)-CI_{\nu,\mathrm{ISRF}}(\lambda)]r\,\mathrm{d}r. \tag{A3}$$

In AM, the equations (A2)–(A6) are employed only for the ext shell. The functions $G(\lambda_i, \lambda)$ represent the normalized spectral response function at the *IRAS* bands, centred at λ_i. The function $S(\lambda, r, \theta)$ is the normalized beam pattern. For our purpose, we have used angle-independent beam patterns given by

$$S(\lambda, r, \theta)=S(\lambda, r)=\left(\frac{1}{2\pi\sigma_\lambda^2}\right)\mathrm{e}^{-r^2/2\sigma_\lambda^2}, \tag{A4}$$

for a Gaussian beam, and

$$S(\lambda, r, \theta)=S(\lambda, r)=\left(\frac{1}{2\pi\sigma_\lambda^2}\right)\delta(r-\sigma_\lambda), \tag{A5}$$

for a uniform beam corresponding to a step function of width $2\sigma_\lambda$, where $\delta(r-\sigma_\lambda)=1$ for $|r|<\sigma_\lambda$, and $\delta(r-\sigma_\lambda)=0$ for $|r|>\sigma_\lambda$. The quantity $\sigma_\lambda=(r_{\mathrm{b},\lambda}/R)$, where R is the radius of the source and $r_{\mathrm{b},\lambda}$ is the radius of the beam at the source for a given λ. To perform an accurate spatial convolution we need values of $I(\lambda, r, \theta)$ on a fine (r, θ) mesh. These are calculated by a two-dimensional interpolation on the pre-computed $I(\lambda, P)$. The expression

$$P=[r^2+p^2-2rp\,\cos(\pi-\theta)]^{1/2}, \tag{A6}$$

where p is the apparent distance of the beam centre from the centre of the visible disc, is useful for this purpose. In order to get $\tilde{I}(\lambda, p)$ we need to perform spatial convolutions on a large number of frequency points in each wavelength band characterized by λ_i. Since performing accurate spatial convolution is computationally expensive and the actual wavelength dependence of the beam sizes is not accurately known (it depends on instrumental characteristics), we assume $[\sigma_\lambda]_i=\sigma_{\lambda_i}(\lambda/\lambda_i)$, $i=1$–4, based on a diffraction limited wavelength dependence. It is a good approximation to assume that, in a given bandwidth $[A_{\lambda_i}, B_{\lambda_i}]$, the beam

width remains constant. We have also assumed that $[\sigma_\lambda]_i = \sigma_{\lambda_i}$, $i = 1$–4. With these two assumptions, the order of integration (spatial + spectral) can be 'reversed' to obtain the (spectral + spatial) convolution integral (see equations A2 and A3). Computationally this has great advantages, since we now need to perform only four spatial convolutions ($i = 1$–4) to get $\tilde{I}(\lambda_i, p)$ at any one beam position p on the disc, instead of hundreds of spatial convolutions to be performed for each p. The interstellar radiation field is given by $I_{\nu,\mathrm{ISRF}}(\lambda) = 4F_{\nu,\mathrm{ISRF}}(\lambda)$, using values appropriate for the solar neighbourhood as a first approximation.